

Review

A Review of Persulfate Activation by Magnetic Catalysts to Degrade Organic Contaminants: Mechanisms and Applications

Ke Tian, Fengyin Shi, Menghan Cao, Qingzhu Zheng and Guangshan Zhang * 

College of Resource and Environment, Qingdao Engineering Research Center for Rural Environment, Qingdao Agricultural University, Qingdao 266109, China

* Correspondence: gszhanghit@gmail.com or gszhang@qau.edu.cn; Tel./Fax: +86-532-5895-7461

Abstract: All kinds of refractory organic pollutants in environmental water pose a serious threat to human health and ecosystems. In recent decades, sulfate radical-based advanced oxidation processes (SR-AOPs) have attracted extensive attention in the removal of these organic pollutants due to their high redox potential and unique selectivity. This review first introduces persulfate activation by magnetic catalysts to degrade organic contaminants. We present the advances and classifications in the generation of sulfate radicals using magnetic catalysts. Subsequently, the degradation mechanisms in magnetic catalysts activated persulfate system are summarized and discussed. After an integrated presentation of magnetic catalysts in SR-AOPs, we discuss the application of persulfate activation by magnetic catalysts in the treatment of wastewater, landfill leachate, biological waste sludge, and soil containing organic pollutants. Finally, the current challenges and perspectives of magnetic catalysts that activated persulfate systems are summarized and put forward.

Keywords: magnetic catalysts; persulfate activation; radical pathway; non-radical pathway; mechanism and application



Citation: Tian, K.; Shi, F.; Cao, M.; Zheng, Q.; Zhang, G. A Review of Persulfate Activation by Magnetic Catalysts to Degrade Organic Contaminants: Mechanisms and Applications. *Catalysts* **2022**, *12*, 1058. <https://doi.org/10.3390/catal12091058>

Academic Editor: Wenhui Wang

Received: 28 August 2022

Accepted: 13 September 2022

Published: 16 September 2022

Publisher's Note: MDPI stays neutral with regard to jurisdictional claims in published maps and institutional affiliations.



Copyright: © 2022 by the authors. Licensee MDPI, Basel, Switzerland. This article is an open access article distributed under the terms and conditions of the Creative Commons Attribution (CC BY) license (<https://creativecommons.org/licenses/by/4.0/>).

1. Introduction

In recent decades, with the rapid development of industry and agriculture, the pollution and treatment of water has become a global problem [1,2]. Some wastewater containing emerging pollutants such as antibiotics, dyes, chlorinated organic pollutants, endocrine-disrupting chemicals, and phenolics have especially caused serious environmental problems due to being irregularly discharged into the environmental medium [3–9]. These emerging pollutants have the characteristics of persistence and low biodegradability, and are difficult to be effectively removed by traditional physical or biological methods, causing serious threats to human health and ecosystems [10–12]. As an effective method of wastewater treatment, advanced oxidation processes (AOPs) play a very important role in water treatment because they can produce radicals with strong redox potential, such as hydroxyl radical ($\cdot\text{OH}$), sulfate radical ($\text{SO}_4^{\cdot-}$), etc., that lead to the degradation of pollutants [13–16].

Fenton oxidation and persulfate oxidation, as representative oxidation methods of AOPs, play an important role in the treatment of wastewater containing refractory organic pollutants. Fenton oxidation, as one of the traditional oxidation methods, has relatively high redox potential [1.8–2.7 V vs. Normal Hydrogen Electrode (NHE)] [17], which is simple to operate and does not consume energy. However, the Fenton system has some limitations, including narrow pH work range, metal ion leaching, and that hydrogen peroxide is unstable and not conducive to storage [18–20]. At present, sulfate radical-based advanced oxidation processes (SR-AOPs) have been favored by many researchers in recent decades because they have better advantages than Fenton processes. Compared with hydroxyl radical, sulfate radical has higher redox potential (2.5–3.1 V vs. NHE), longer half-life (30–40 μs vs. 20 ns), and a wider pH operating range (2~8) [21,22]. In addition, sulfate radical is selective and can preferentially attack the designated group to degrade organic pollutants

quickly and efficiently [23]. Therefore, SR-AOPs play an increasingly important role in water treatment. Generally, there are two sources of $\text{SO}_4^{\cdot-}$ production: permonosulfate (PMS) and peroxydisulfate (PDS). PMS is a compound salt ($2\text{KHSO}_5 \cdot \text{KHSO}_4 \cdot \text{K}_2\text{SO}_4$), and the trade name is oxyone [24]; PDS can be divided into sodium salt, potassium salt, and ammonium salt. Among them, sodium persulfate is commonly used as peroxydisulfate due to its stability and ease of transportation and storage [25]. PDS and PMS are not reactive at room temperature and it is hard for them to decompose by themselves [26], but can be activated by different means to produce sulfate radicals, such as transition metal ions, metal oxides, microwaves (MWs), ultraviolet light (UV), ultrasonic (US), etc., which are good persulfate activators [27–31].

However, activation of persulfate by transition metal ions causes ion leaching problems that results in secondary pollution, and could precipitate under alkaline conditions, which makes the degradation process complicated [20]. Therefore, the activation of persulfate gradually changes from a homogeneous system to a heterogeneous system. Generally, although a heterogeneous catalyst does not consume energy and the operation is simple, the recovery of catalyst is difficult and requires centrifugation or filtration [32]. Therefore, the synthesis of a magnetic catalyst becomes increasingly advantageous. On the one hand, the magnetic catalyst activates persulfate to produce an active species by electron transfer, which does not consume energy, so it can be regarded as a green catalyst. On the other hand, the magnetic catalyst can be easily recovered by the magnet without centrifugation or precipitation, which greatly saves the processing time and cost, making it an ideal persulfate activation material. For instance, Yin et al. [33] synthesized magnetic reduced graphene- Fe_3O_4 (rGO- Fe_3O_4) composite for persulfate activation by a coprecipitation method, which has good norfloxacin (NOR) removal performance; Hu et al. [34] used magnetic Fe_3O_4 in connection with a microwave to activate PDS to achieve enhanced degradation of *p*-nitrophenol (PNP); Cui et al. [35] synthesized a magnetic nano Fe_3O_4 -BC catalyst via a coprecipitation method to activate PMS, demonstrating excellent catalytic stability for bisphenol A removal. Magnetic materials are easy to recover and have been paid more attention as an effective recovery method in the exploration and application of persulfate activation in related research fields.

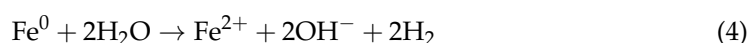
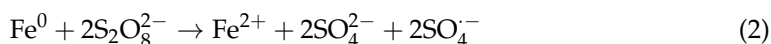
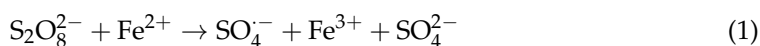
In this paper, we first introduce different kinds of magnetic catalysts for persulfate activation to degrade refractory organic pollutants. In addition, the degradation mechanism of magnetic catalysts activated persulfate system is summarized and discussed. Then, the applications of the system in wastewater, landfill leachate, biological waste sludge, and soil containing refractory organic pollutants are introduced. Finally, the problems and future prospects of magnetic materials activated persulfate are presented, hoping to make some contributions to SR-AOPs.

2. Magnetic Catalysts for Persulfate Activation

2.1. Zero-Valent Iron (ZVI, Fe^0)

To avoid the secondary pollution caused by ferrous ions (Fe^{2+}), zero-valent iron, as a green source of Fe^{2+} , plays an important role in the activation of persulfate (Equation (1)) [36]. In addition, ZVI has good ferromagnetism, which is easy to recover from the degradation system and greatly reduces the treatment cost. Specifically, there are two ways for ZVI to activate persulfate. On the one hand, as a strong reducing agent, ZVI can directly reduce persulfate through an electron transfer pathway to produce sulfate radicals (Equation (2)) [37]; on the other hand, ZVI activates persulfate via slowly and smoothly releasing Fe^{2+} through corrosion under aerobic or anaerobic conditions (Equations (3) and (4)) [38,39]. In addition, for ferric ions (Fe^{3+}) produced in the activation of persulfate by Fe^{2+} , the reduction of ZVI can reduce Fe^{3+} to Fe^{2+} (Equation (5)), thus forming a stable cycle of $\text{Fe}^{2+}/\text{Fe}^{3+}$, effectively activating persulfate to produce sulfate radicals and promoting the effective degradation

of pollutants [25,40]. Furthermore, the reaction of Fe^{3+} and ZVI can effectively avoid the hydrolysis and precipitation made by the accumulation of Fe^{3+} [20].



There are many studies on the activation of persulfate by ZVI. For instance, Palharim et al. [41] explored two advanced oxidation processes: UV/persulfate system and ZVI/persulfate system, and found that ZVI can effectively activate persulfate and achieve more than 97.5% removal of propylparaben. Among them, sulfate radicals played a dominant role. Similarly, Hayat et al. [42] found that the nano-ZVI/PDS system can effectively remove 96.6% imidacloprid (IMI) while exploring the removal effect of magnetic biological carbon, nano-ferric oxide, and nano-ZVI on IMI by activating PDS, respectively. However, the difference is that $\cdot\text{OH}$ is the main active species in the system.

However, these studies showed that the reduction of the pollutant removal rate was limited by the continued increase of ZVI dosage, because the excess active species would undergo a self-quenching reaction in the system, thus affecting its degradation efficiency.

2.2. Iron Oxide

Iron oxides have a variety of different oxidation forms, such as hematite, goethite, magnetite, pyrite, etc., and are good persulfate activator [43–46]. Because of excellent ferromagnetism, iron oxides are easy to separate and recover from the solution. The principle of persulfate activation is similar to that of zero-valent iron. Through the gradual release of Fe^{2+} from the surface of iron oxide into the solution, persulfate can be activated to produce active species and then participate in redox reaction [34]. In recent decades, Fe_3O_4 has a good application prospect in activated persulfate. For example, Zhao et al. [47] synthesized magnetic Fe_3O_4 by a coprecipitation method, and the Fe_3O_4 /PDS system can completely remove p-nitroaniline at neutral pH. Yan et al. [48] synthesized magnetic Fe_3O_4 by a reverse coprecipitation method, which completely removed 0.06 mmol/L sulfamethoxine in 15 min. The degradation process produced harmless intermediates, which can be considered as a green persulfate oxidant.

In addition, other iron oxides can also be used as excellent activators of persulfate. Hussain et al. [49] synthesized a magnetic BiFeO_3 nano-catalyst by a sol-gel method, which can effectively activate persulfate to remove aniline. Sulfate radicals and hydroxyl radicals are the main active species in the system. In addition, the repeated experiments indicated that the material has high stability, which can still remove 93.3% aniline in the solution after five recycling cycles. Guan et al. [50] synthesized magnetic copper ferrite (CuFe_2O_4) by a sol-gel method to activate persulfate, and the system can remove more than 98% of atrazine within 15 min.

Iron oxides come in various forms and they are easily recovered because of their magnetic properties. In addition, they can also be used as a green catalytic material, which can be further explored in the activation of persulfate.

2.3. Nickel-Cobalt Bimetallic Catalyst

Transition metal cobalt ion is one of the effective activators of PDS, but due to its high leaching concentration, it is easy to cause secondary pollution, which is harmful to the ecosystem and requires further treatment. In recent years, as a low-cost, magnetically separable catalyst, nickel-cobalt bimetallic catalyst has a certain application prospect in the activation of persulfate. Tian et al. [51] prepared dandelion NiCo_2O_4 microspheres by

the hydrothermal method, which has a good mesoporous structure and can effectively activate persulfate to degrade humic acid (HA). The introduction of Ni effectively reduces the toxicity of Co and can be considered as a green catalyst for environmental protection. Wu et al. [52] synthesized a NiCo_2O_4 catalyst with a porous network structure to activate PMS to degrade tetracycline (TC) and bisphenol A (BPA). The high catalytic performance can be attributed to the covalent conversion between $\text{Ni}^{2+}/\text{Ni}^{3+}$ and $\text{Co}^{2+}/\text{Co}^{3+}$ (Figure 1).

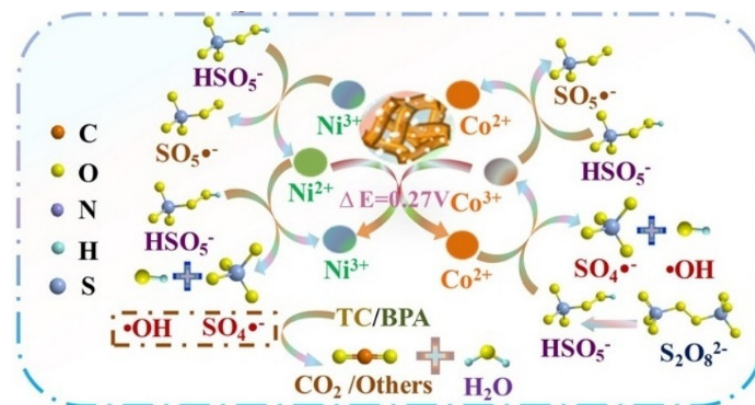


Figure 1. The recycle of $\text{Ni}^{2+}/\text{Ni}^{3+}$ and $\text{Co}^{2+}/\text{Co}^{3+}$ and the removal mechanism of TC and BPA in the $\text{NiCo}_2\text{O}_4/\text{PMS}$ system [52].

In addition, as a magnetic carrier, nickel foam can be easily recovered from the reaction solution. Hu et al. [53] used a microwave-assisted method to load $\text{Co}_3\text{O}_4\text{-Bi}_2\text{O}_3$ nanoparticles on the nickel foam carrier to degrade BPA via persulfate activation. The excellent catalytic activity came from the electron transfer between $\text{Co}^{2+}/\text{Co}^{3+}$, $\text{Bi}^{3+}/\text{Bi}^{5+}$ and $\text{Ni}^{2+}/\text{Ni}^{3+}$, realizing the continuous regeneration of active species, and 95.6% of BPA was removed within 30 min.

2.4. Supported Magnetic Catalyst

However, a common problem with the magnetic materials mentioned above is that they are easy to aggregate [54]. Therefore, researchers are increasingly interested in loading magnetic materials onto various forms of biochar carriers to produce magnetic biocarbon materials [32,55,56]. On the one hand, the aggregation of nanomaterials can be reduced; on the other hand, the advantages of carbonaceous materials can be fully exploited, and the synergistic effect of the nanomaterials and carbonaceous materials can be well applied to the removal of organic pollutants [57]. There are abundant sources of carbon materials in nature, many of which exist in the form of wastes [54]. The secondary utilization of carbon through high-temperature calcination or pyrolysis can effectively realize the resource utilization of wastes [58].

Abundant forms of carbon provide a variety of carrier forms for magnetic materials, so kinds of magnetic carbon materials with high efficiency in activating persulfate were developed. Fu et al. [59] used *Myriophyllum aquaticum* composites as a carbon source, and prepared a Fe_3O_4 -porous biological carbon ($\text{Fe}_3\text{O}_4\text{-MC}$) catalyst with a highly graphitized structure, multi-porous structure (homogeneous distribution of mesopores and micropores), and strong magnetic properties through high temperature pyrolysis. At the pyrolysis temperature of 800 °C, $\text{Fe}_3\text{O}_4\text{-MC}$ can effectively activate PMS and completely remove *p*-hydroxybenzoic acid (HBA) within 30 min. Yin et al. [33] prepared a nanosheet reduced rGO- Fe_3O_4 catalyst by a coprecipitation method. After four recycling cycles, the rGO- $\text{Fe}_3\text{O}_4/\text{PDS}$ system can still remove 74.99% of NOR (Figure 2a), and the XRD characteristic diffraction peaks before and after the reaction do not change significantly (Figure 2b), indicating that the material has good stability. Zhang et al. [56] used ferrocene and carbon nanofibers (CNFs) as precursors, and prepared carbon-encapsulated Fe_3O_4 ($\text{Fe}_3\text{O}_4@\text{C}/\text{CNFs}$) magnetic materials on carbon nanofibers. The CNF carrier effectively

avoids the agglomeration of Fe_3O_4 , and the leaching amount of iron ions after five recycling cycles is very low, which is about 1/20 of the leaching amount of iron ions in commercial Fe_3O_4 under the same conditions.

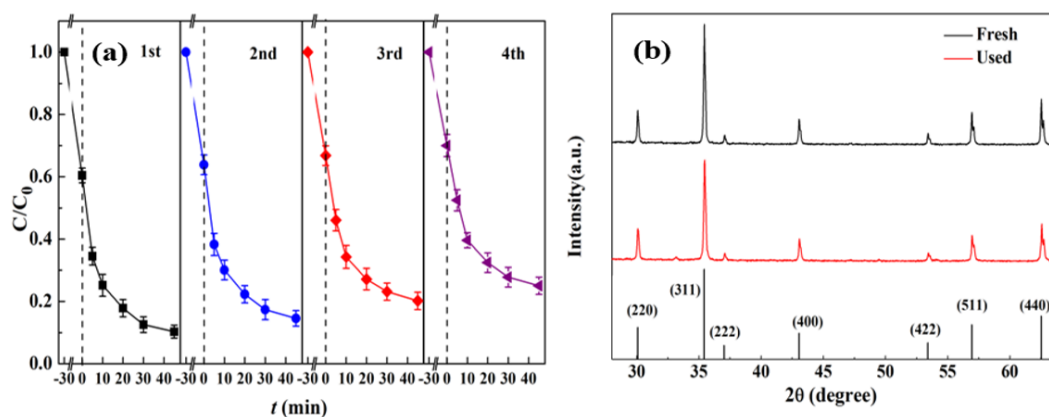


Figure 2. Recycling experiment of rGO- Fe_3O_4 (a) and XRD patterns of the fresh and used rGO- Fe_3O_4 (b) [33].

Generally, iron, cobalt, and nickel are the three main transition metals in magnetic materials, and the existence of a carrier is beneficial to the aggregation of nanoparticles. In addition, magnetic materials have bright prospects in persulfate activation due to their excellent recovery ability, simple operation, and energy saving.

3. Mechanism for Persulfate Activation by Magnetic Catalysts

In SR-AOPs, the reactive oxygen species (ROS) produced in persulfate systems vary with catalysts and target pollutants. According to the nature of active species, the activation mechanism of persulfate can be divided into a radical pathway and non-radical pathway. The main radical pathways are sulfate radicals, hydroxyl radicals, and superoxide anion radicals; non-radical pathways mainly include electron transfer pathways, singlet oxygen, and complexes formed by catalytic materials and persulfate adsorbed on them during the reaction. Therefore, it is important to identify these active species during the reaction first.

3.1. Identification of Reactive Oxygen Species

Two methods are commonly used to explore ROS in the system: (1). quenching experiments; (2). electron paramagnetic resonance (EPR) or electron spin resonance (ESR). In the quenching experiment, a certain amount of quench agents are added to the system to react with the corresponding active species, and the existence of the active species is judged according to the inhibition effect on the degradation of targeted pollutants. The identification of the active species is determined by the reaction rate constant (k_{obs}) between the quenching agent and the active species (Table 1). For common quenching agents, both methanol (MeOH) and ethanol (EtOH) can be used to identify $\text{SO}_4^{\cdot-}$ and $\cdot\text{OH}$, and tert-butanol (TBA) can be used to identify $\cdot\text{OH}$ [60–64]. Since MeOH, EtOH, and TBA are hydrophilic and tend to react with active species in solution, potassium iodide (KI) and phenol are used to identify $\text{SO}_4^{\cdot-}$ and $\cdot\text{OH}$ on the surface of materials, and nitrobenzene (NB) is used to identify $\cdot\text{OH}$ on the surface of catalyst materials [59,61,65–69]. Para-benzoquinone (*p*-BQ) is used to identify $\text{O}_2^{\cdot-}$ [66,70]. Both furfuryl alcohol (FFA), L-Listidine, and sodium azide (NaN_3) can be used to selectively react with $^1\text{O}_2$ [66,71–75]. In addition, the reduction of Zeta potential could affect the electrostatic binding between solute and suspended solid in solution, and thus hinder the electronic transfer of organic pollutants to the catalyst to a certain extent. However, the presence of NaClO_4 will reduce the Zeta potential of the catalyst [59,68,76]. Therefore, adding NaClO_4 to the reaction system can identify e^- .

Table 1. The reaction rate constants of commonly used quenching agents with active species.

Quench Agents	Targeted ROS	Reaction Rate Constants (M ⁻¹ ·s ⁻¹)	Identification of ROS	Location of ROS	Ref.	
MeOH	SO ₄ ^{·-}	3.2 × 10 ⁶	SO ₄ ^{·-} , ·OH	In the solution	[60–62]	
	·OH	9.7 × 10 ⁸				
TBA	SO ₄ ^{·-}	4–9.1 × 10 ⁵	·OH	In the solution		
	·OH	3.8–7.6 × 10 ⁸				
EtOH	SO ₄ ^{·-}	1.6–7.7 × 10 ⁷	SO ₄ ^{·-} , ·OH	In the solution		[63,64]
	·OH	1.2–2.8 × 10 ⁸				
Phenol	SO ₄ ^{·-}	8.8 × 10 ⁹	SO ₄ ^{·-} , ·OH	Catalyst surface	[65,66]	
	·OH	6.6 × 10 ⁹				
KI	SO ₄ ^{·-}	-	SO ₄ ^{·-} , ·OH	Catalyst surface	[61,67]	
	·OH	-				
NB	SO ₄ ^{·-}	<10 ⁶	·OH	Catalyst surface	[59,68,69]	
	·OH	3.9 × 10 ⁹				
<i>p</i> -BQ	O ₂ ^{·-}	1.0 × 10 ⁹	O ₂ ^{·-}	Catalyst surface	[66,70]	
L-listidine		3.2 × 10 ⁷			[71,72]	
FFA	¹ O ₂	1.2 × 10 ⁸	¹ O ₂	-	[73,74]	
NaN ₃		1.0 × 10 ⁹			[66,75]	
NaClO ₄	e ⁻	-	e ⁻	-	[59,68,76]	

Another method is electron paramagnetic resonance (EPR) or electron spin resonance (ESR). Direct detection with EPR or ESR is difficult due to the relatively short life span of active species. Therefore, spin capture agents are added to combine with active species to form relatively stable spin admixtures, which are converted into paramagnetic species easily measured by EPR or ESR [77]. For SO₄^{·-}, ·OH and O₂^{·-}, 5,5-dimethyl-1-pyrroline-1-oxide (DMPO) is generally selected as the optional trapping agent, thus forming DMPO-SO₄^{·-}, DMPO-·OH, and DMPO-O₂^{·-} spin admixtures [56,59,78]; ¹O₂ can be captured by 2,2,6,6-tetramethyl-4-piperidine (TEMP) to form the spin adduct TEMP-¹O₂ [79]. After the adducts are obtained, hyperfine splitting constants (HPC) are calculated using specialized software related to EPR technology, and these constants are then compared with databases or the literature to identify active species [77].

As shown in Figure 3, for the DMPO-·OH adduct, it generally presents a quaternion characteristic peak of 1:2:2:1 (HPC:α_N = 14.9 G, α_{β-H} = 14.9 G) (Figure 3a) [77,80]; for DMPO-SO₄^{·-} admixtures, the characteristic peaks generally show a six-component characteristic peak of 1:1:1:1:1:1 (HPC:α_N = 13.51 G, α_{β-H} = 9.93 G, α_{γ-H1} = 1.34 G, α_{γ-H2} = 0.88 G) (Figure 3a) [77,80]. It is worth noting that some studies have found that quenching experiments proved the existence of SO₄^{·-}, ·OH, but no corresponding characteristic peak was found in EPR. However, a seven-element peak of 1:2:1:2:1:2:1 appeared due to the oxidation of DMPO by oxidizing species (SO₄^{·-}, ·OH) into a special admixture DMPO-X, which can also explain the existence of SO₄^{·-}, ·OH (Figure 3b) [59,81]. For DMPO-O₂^{·-} admixtures, the characteristic peaks generally show a six-component characteristic peak of 1:1:1:1:1:1 (HPC:α_N = 14.3 G, α_{β-H} = 11.2 G, α_{γ-H1} = 1.3 G) (Figure 3c) [77,82]. For the TEMP-¹O₂ adduct, it generally presents a ternary characteristic peak of 1:1:1 (HPC:α_N = 16.3 G) (Figure 3d) [77,82].

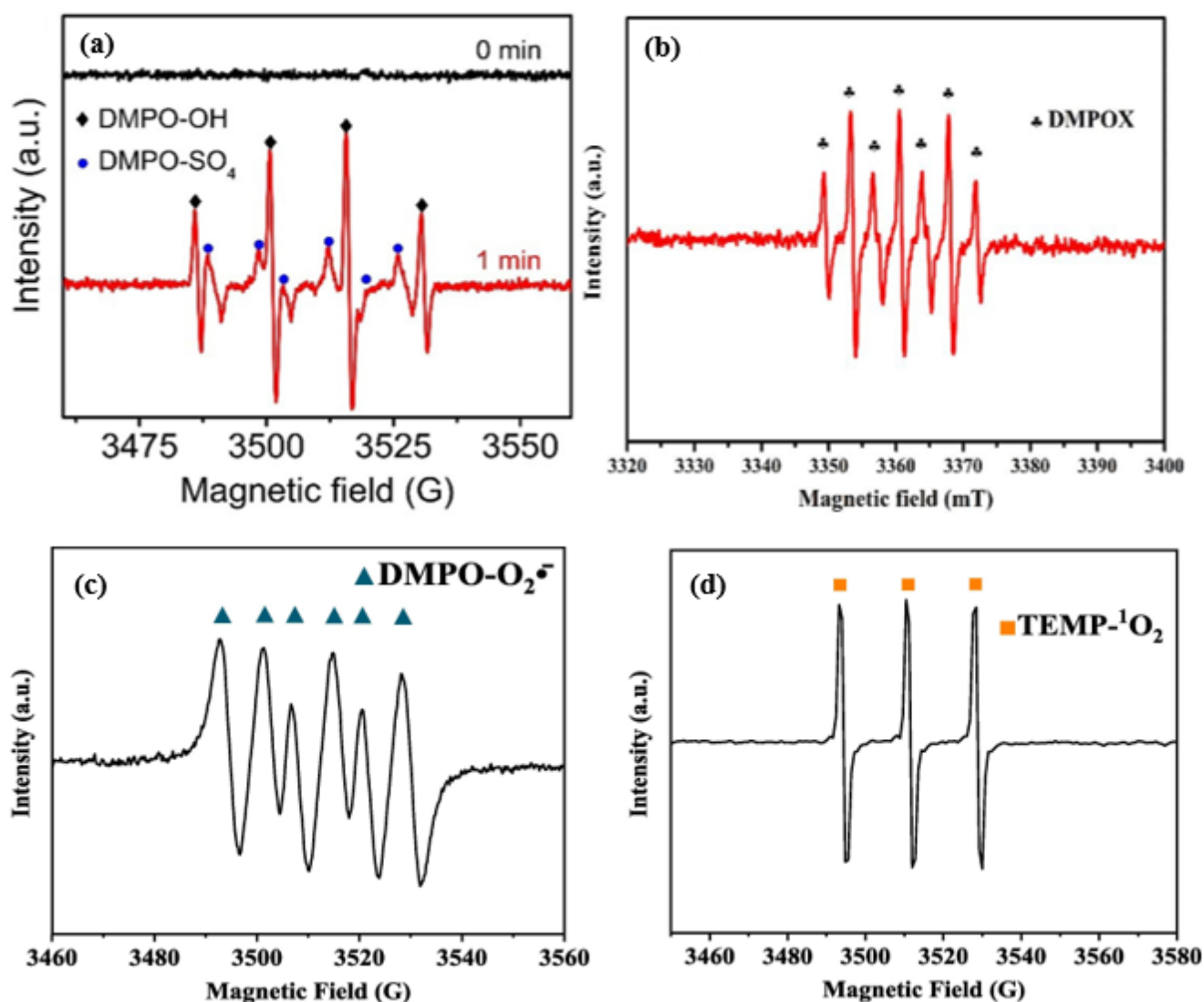


Figure 3. EPR characteristic spectrum of (a) DMPO-SO₄^{•−} and DMPO-·OH; (b) DMPO-X; (c) DMPO-O₂^{•−}; and (d) TEMP-¹O₂ [80–82].

In general, the combination of the quenching experiment and EPR/ESR can strongly explain the active species in the system and provide strong support for the activation mechanism of persulfate. Therefore, when exploring the activation mechanism in the reaction process, it is necessary to combine the above two kinds of active species identification methods as far as possible, to make the article more scientific and rigorous.

3.2. Radical Pathway and Non-Radical Pathway

In persulfate systems, different catalysts play different roles with persulfates and have different activation mechanisms. Some are based on the radical pathway, some are based on the non-radical pathway, and some combine the radical pathway with the non-radical pathway. Here, the following section will be introduced, respectively, and some active species involved in the reaction process were summarized in Table 2 [33–35,37,53,55,59,79,83–93].

Table 2. Active species involved in the reaction process.

Reaction Pathway	System	Targeted Pollutant	pH	Quenching Agent (Degradation Rate after Inhibition, Control Degradation Rate)	EPR Signal	Activation Mechanism	Ref.
Radical pathway	Fe ₃ O ₄ -BC/PMS	BPA	3.0	TBA (84.5%, 100%) EtOH (47.6%, 100%)	DMPO-X	SO ₄ ^{•-} (major), •OH	[35]
	nZVI-Omt/PDS	SMZ	6.8	TBA (73%, 97%) MeOH (40%, 97%)	DMPO-•OH DMPO-SO ₄ ^{•-}	SO ₄ ^{•-} , •OH	[37]
	nZVI-BC/PDS	TC	5.0	TBA (75.95%, 87.58%) EtOH (32.65%, 87.58%)	DMPO-•OH DMPO-SO ₄ ^{•-}	SO ₄ ^{•-} (major), •OH	[83]
	Co ₃ O ₄ -CeO ₂ /PDS	TC	7	TBA (52%, 79%) MeOH (41%, 79%)	DMPO-•OH DMPO-SO ₄ ^{•-}	SO ₄ ^{•-} , •OH(major)	[84]
	Co ₃ O ₄ - Bi ₂ O ₃ @NF/PMS	BPA	3.4	TBA (~95%, 95.6%) MeOH (~95%, 95.6%) KI (~8%, 95.6%)	DMPO-•OH DMPO-SO ₄ ^{•-}	SO ₄ ^{•-} surface, •OH _{surface}	[53]
	Ag _{0.4} -BiFeO ₃ /PDS	TC	4.5	TBA (~48%, 91%) MeOH (~52%, 91%)	DMPO-•OH DMPO-SO ₄ ^{•-}	SO ₄ ^{•-} , •OH(major)	[85]
	Fe ₃ O ₄ @CuO _x /PDS	sulfadiazine (SDZ)	7	TBA (58.6%, 95%) MeOH (18.2%, 95%)	DMPO-•OH DMPO-SO ₄ ^{•-}	SO ₄ ^{•-} (major), •OH	[86]
	Fe ₃ O ₄ /hf- CuO/PDS	4- aminobenzenesulfonic acid (4-ABS)	7	TBA (45.7%, 90%) MeOH (4.3%, 90%)	DMPO-•OH DMPO-SO ₄ ^{•-}	SO ₄ ^{•-} , •OH	[87]
	Fe ₃ O ₄ /MW/PDS	PNP	3.4	TBA (76.2%, 98.2%) MeOH (29.3%, 98.2%)	DMPO-•OH DMPO-SO ₄ ^{•-}	SO ₄ ^{•-} (major), •OH	[34]
Non-radical pathway	RC/CNTs/Fe ₃ O ₄ NPs/PDS	BPA	6.07	TBA (~100%, 100%) EtOH (~100%, 100%) FFA (~60%, 100%)	TEMP- ¹ O ₂	¹ O ₂ , electron transfer, catalyst-PDS *	[55]
	rGO-Fe ₃ O ₄ /PDS	NOR	6.47	TBA (~82%, 89.6%) EtOH (~73%, 89.6%) FFA (~50%, 89.6%)	-	¹ O ₂ , electron transfer	[33]
	Ni-NiO/PDS	4-CP	7.0	MeOH (~80%, 100%) (The removal of FFA is lower than 10%)	-	Electron transfer	[88]
	Co ₃ O ₄ @NCNTs/PDS	Orange G (OG)	7.0	TBA (90.1%, 100%) EtOH (~90%, 100%) FFA (17.3%, 100%) <i>p</i> -BQ (~70%, 100%)	DMPO-•OH DMPO-SO ₄ ^{•-} DMPO-O ₂ ^{•-} TEMP- ¹ O ₂ (major)	¹ O ₂ (major), electron transfer, catalyst-PDS *	[89]
	UBC- <i>x</i> /PMS	BPA	6.84	TBA (~100%, 100%) EtOH (~100%, 100%) FFA (75%, 100%)	DMPO-•OH DMPO-SO ₄ ^{•-} DMPO-O ₂ ^{•-} TEMP- ¹ O ₂	¹ O ₂ (major)	[90]

Table 2. Cont.

Reaction Pathway	System	Targeted Pollutant	pH	Quenching Agent (Degradation Rate after Inhibition, Control Degradation Rate)	EPR Signal	Activation Mechanism	Ref.
Radical pathway and non-radical pathway	Fe ₃ O ₄ /MC/PMS	HBA	-	Phenol (10%, 100%) NB (88%, 100%) <i>p</i> -BQ (67%, 100%) NaClO ₄ (70%, 100%) TBA (56.9%, 98.2%) MeOH (44.6%, 98.2%)	DMPO-X	SO ₄ ^{·-} _{-surface} , ·OH, O ₂ ^{·-} , electron transfer	[59]
	Fe-N-BC/PDS	acid orange (AO7)	7.0	KI (~30%, 98.2%) FFA (~68%, 98.2%) BQ (~35%, 98.2%)	DMPO-·OH DMPO-SO ₄ ^{·-} DMPO-O ₂ ^{·-} TEMP- ¹ O ₂	SO ₄ ^{·-} , ·OH, O ₂ ^{·-} , ¹ O ₂ , electron transfer, catalyst-PDS *	[79]
	FeCN _x /PMS	BPA	6.5	MeOH (~90%, 94%) KI (~42%, 94%) NaN ₃ (~16%, 94%)	DMPO-·OH DMPO-SO ₄ ^{·-} TEMP- ¹ O ₂	SO ₄ ^{·-} _{-surface} , ·OH _{-surface} , ¹ O ₂ , electron transfer, catalyst-PMS *	[91]
	Fe ₃ O ₄ / CoCO ₃ /rGO/PMS	Rhodamine B (RhB)	7.0	TBA (72.5%, 98.69%) EtOH (10.29%, 98.69%) FFA (complete inhibition)	-	SO ₄ ^{·-} (major), ¹ O ₂ (major), ·OH	[92]
	nZVI@NBC/PDS	BPA	7.0	TBA (77.3%, 100%) EtOH (74.1%, 100%) FFA (12%, 100%)	DMPO-·OH DMPO-SO ₄ ^{·-} TEMP- ¹ O ₂	SO ₄ ^{·-} , ·OH, ¹ O ₂	[93]

Note: "*" represents the complex formed between the catalyst and the oxidant adsorbed on its surface.

3.2.1. Radical Pathway

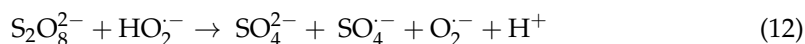
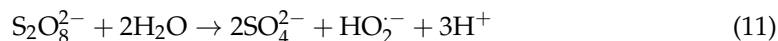
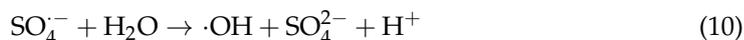
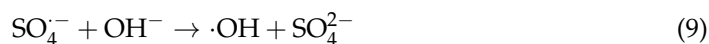
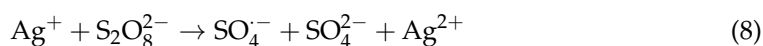
In persulfate systems, persulfates are activated by magnetic catalysts to produce $\text{SO}_4^{\cdot-}$, $\cdot\text{OH}$, and $\text{O}_2^{\cdot-}$ (Equations (6)–(12)) [10,94,95]. Due to its strong redox ability, $\text{SO}_4^{\cdot-}$, $\cdot\text{OH}$ and $\text{O}_2^{\cdot-}$ can act with target pollutants and mineralize them into small molecules.

In most systems, $\text{SO}_4^{\cdot-}$ was the main active species. For example, Cui et al. [35] used a coprecipitate method to synthesize a nano Fe_3O_4 -BC catalyst to activate persulfate, and EtOH and TBA were used to quench $\text{SO}_4^{\cdot-}$ and $\cdot\text{OH}$. The inhibitory effect of EtOH on BPA was significantly higher than that of TBA, and an EPR experiment showed DMPO-X's characteristic peak, indicating that DMPO was oxidized by $\text{SO}_4^{\cdot-}$ and $\cdot\text{OH}$, therefore, the system was dominated by a $\text{SO}_4^{\cdot-}$ -based radical system. Shao et al. [83] synthesized Fe_3O_4 loaded by BC (Fe_3O_4 -BC) to activate PDS to degrade tetracycline. EtOH and TBA were chosen to quench $\text{SO}_4^{\cdot-}$ and $\cdot\text{OH}$. The results showed that the inhibition effect of EtOH on TC was significantly higher than that of TBA. DMPO- $\text{SO}_4^{\cdot-}$ and DMPO- $\cdot\text{OH}$ signals were also detected in the EPR experiment, therefore, the system was also a $\text{SO}_4^{\cdot-}$ dominated radical system.

In addition, $\cdot\text{OH}$ played a major role in some systems, which may be related to the pH of the reaction or the nature of targeted pollutant [84,85]. Ouyang et al. [85] prepared a silver-doped bismuth ferrite composite ($\text{Ag}_{0.4}\text{-BiFeO}_3$) by a sol-gel method, which was used to activate PMS and degrade TC. DMPO- $\text{SO}_4^{\cdot-}$ and DMPO- $\cdot\text{OH}$ signals were detected by ESR, and DMPO- $\cdot\text{OH}$ signals were stronger than DMPO- $\text{SO}_4^{\cdot-}$ signals. To further demonstrate the existence of active species, methanol and tert-butanol were used to quench $\text{SO}_4^{\cdot-}$ and $\cdot\text{OH}$, and the inhibition effect of tert-butanol on TC in the system was slightly weaker than methanol. Therefore, both $\text{SO}_4^{\cdot-}$ and $\cdot\text{OH}$ in an $\text{Ag}_{0.4}\text{-BiFeO}_3$ /PMS system are involved in degradation reactions. Specifically, low-valent transition metal ions activate PMS to produce sulfate radicals, then sulfate radicals react with an H_2O molecule or hydroxide ion in a solution to produce $\cdot\text{OH}$, and $\cdot\text{OH}$ is the main one in the system.

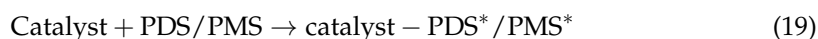
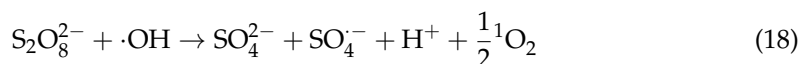
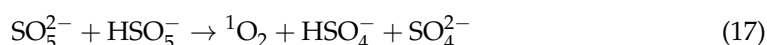
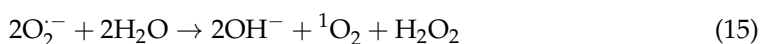
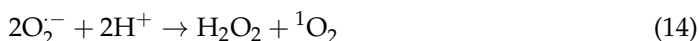
However, not all persulfate systems can be investigated for the presence of radicals by quenching and EPR experiments. In some persulfate systems, other methods have been used by some researchers to demonstrate radical pathway. Guan et al. [50] synthesized copper ferrate catalyst (CuFe_2O_4) to activate PMS to degrade atrazine by a sol-gel method, assuming only $\cdot\text{OH}$ exists in the reaction system. Therefore, the removal of NB and ATZ by CuFe_2O_4 /PMS system was compared, and the contribution of $\cdot\text{OH}$ on the catalyst surface was investigated according to the ratio of quasi-first-order rate constant of reaction kinetics of each system during the degradation process. The results showed that the actual value of the ratio of quasi-first-order rate constants ($k_{\text{ATZ}}/k_{\text{NB}} = 6.4$) is much higher than the theoretical value (0.5~1), which proves that $\text{SO}_4^{\cdot-}$ and $\cdot\text{OH}$ are the main active species on the catalyst surface.

Magnetic catalyst activates persulfate to produce radicals such as $\text{SO}_4^{\cdot-}$, $\cdot\text{OH}$, and $\text{O}_2^{\cdot-}$ with strong oxidation to attack pollutants, and pollutants are broken down into small molecules of inorganic oxide, CO_2 and H_2O in a short time. In general, the radical pathway is an effective way to remove pollutants by AOPs.



3.2.2. Non-Radical Pathway

However, in other persulfate systems, radicals play a very small role, and the removal of pollutants is mainly induced by the non-radical pathway including singlet oxygen, electron transfer, and complex. Generally, there are three production sources of $^1\text{O}_2$: (1). Transformation of superoxide anion radicals (Equations (13)–(15)) [82,96]; (2). The decomposition of persulfates occurs directly (Equations (16)–(18)) [86,92,97,98]; and (3). Transformation of functional groups. For example, because of the existence of the O-O bond, persulfates are easily polarized by catalytic materials with polar structure to produce $^1\text{O}_2$, and $^1\text{O}_2$ can also be induced by the presence of C=O and graphite N according to different catalyst materials, especially the magnetic catalyst with carbon material as the carrier [99,100]. Studies have shown that $^1\text{O}_2$ owns highly selectivity and tends to attack electron-rich organic pollutants such as phenols [101]. Electron transfer pathway also plays an important role in the degradation of pollutants. Generally, catalysts are good electron transfer agents (electron mediators), can transfer electrons from adsorbed organic pollutants (electron donors) to persulfate (electron acceptors), promoting redox reactions [102]. The formation of complexes generally takes place on magnetic catalysts supported by carbon materials. That is, carbon with a positive charge forms a stable complex with high redox capacity due to the strong electrostatic binding force between it and PDS/PMS (catalyst-PDS*, catalyst-PMS*) (Equation (19)) [55,91].



Different from the radical pathway, the activation mechanisms explored in the following systems are mainly induced by the non-radical pathway. For instance, Yin et al. [33] synthesized the rGO-Fe₃O₄ composite catalyst to activate PDS via a coprecipitation method. For the reaction mechanism of NOR, the author found that $^1\text{O}_2$ is the main active species relative to $\text{SO}_4^{\cdot-}$ and $\cdot\text{OH}$ by quenching experiment. The timing of the current analysis showed that the current jump was significant only in the presence of the contaminant NOR, catalyst rGO-Fe₃O₄, and oxidant PDS. This phenomenon demonstrates the existence of an electron transfer pathway from pollutant to catalyst and then to oxidant. Thus, the coexistence of singlet oxygen and electron transfer promoted the degradation of NOR. Kim et al. [88] synthesized a nanocomposite catalyst of nickel metal and nickel oxide (Ni-NiO) by a sol-gel method to activate PDS for the degradation of 4-chlorophenol (4-CP). EPR could not detect the signal of radicals, and methanol was used to quench the possible active species, and there was almost no inhibition on the removal of 4-CP, proving that the reaction was a non-radical pathway. It is worth noting that the Ni-NiO/PDS system has less than 10% removal effect on FFA, which also excludes the effect of $^1\text{O}_2$. Linear sweep voltammetry (LSV) and PDS decomposition experiments showed that Ni-NiO catalyst acts as electron transfer medium and promotes electron transfer from pollutant to PDS. Furthermore, based on the previous studies, the authors hypothesized that Ni-NiO forms reactive complexes with PDS adsorbed on its surface, leading to activation of PDS and oxidation of contaminants in the system.

Similarly, through a series of electrochemical signal experiments, Lai' team also found that the removal of pollutants in the persulfate system was based on the generation of complex as the main oxidative species [55]. Specifically, the team synthesized magnetic renewable fiber-loaded carbon nanotubes/ferric oxide nanocomposites (RC/CNTs/Fe₃O₄

NPs) to activate PDS and degrade BPA. Two electrochemical characterization methods, electrochemical impedance spectroscopy (EIS) and Tafel polarization curve, verified the existence of electron transfer pathway (Figure 4a,b). The existence of the complex was also proven by electrochemical experiments as well. First, catalyst and oxidizer combined to form catalyst-PDS*, and the composite material transfers some electrons to PDS, which leads to the increase of oxidation potential of catalyst-PDS*. When a new equilibrium is reached, BPA was added, and catalyst-PDS* accepts electrons from BPA, thus reducing the oxidation potential. Then, the oxidation potential of catalyst-PDS* increased when the content of BPA decreased with degradation. Finally, when the content of BPA decreased with degradation, the oxidation potential of catalyst-PDS* rose again. Here, when BPA was added again, the oxidation potential of catalyst-PDS* decreased first and then rose again, which proved the existence of catalyst-PDS* complex (Figure 4c). In addition, the quenching and EPR experiments showed that $^1\text{O}_2$ was the main oxidizing species. Hence, $^1\text{O}_2$, together with the electron transfer pathway and the formation of the complex promoted the degradation of BPA (Figure 4d).

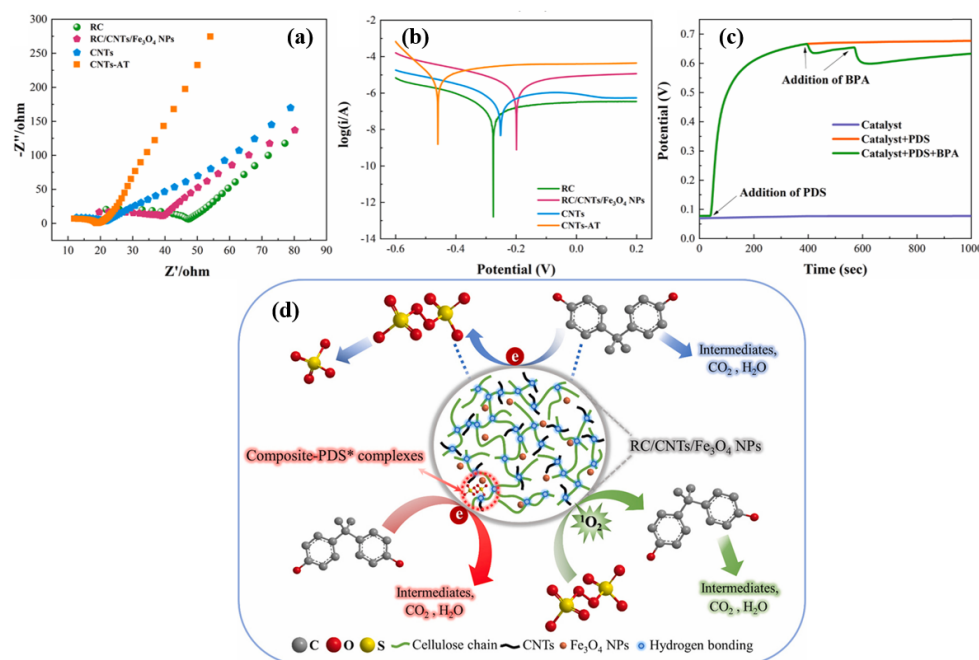


Figure 4. Electrochemical impedance spectroscopy. (a) Tafel polarization curve; (b) the open circuit potential curve (c) and schematic diagram of the mechanism (d) of the BPA removal in the RC/CNTs/Fe₃O₄/PDS system [55].

Reaction mechanisms dominated by the non-radical pathway are gaining increasing attention in persulfate-based advanced oxidation processes because of their ability to overcome some of the limitations of radical activation (such as short half-lives). Although the non-radical pathway does not directly rely on strong oxidation to attack pollutants (except $^1\text{O}_2$), it also promotes the redox reaction by forming a complex with strong oxidation or by electron transfer in the reaction system, causing the degradation of pollutants. It is worth noting that the non-radical pathway is not a single one at work, but may involve two or more pathways, which is worth noting when exploring the activation mechanism of persulfate.

3.2.3. The Synergetic Radical Pathway and Non-Radical Pathway

Under the activation of some composite catalyst, the method of persulfate degradation of pollutants diversification involves the radical approaches containing sulfate radicals, hydroxyl radicals, superoxide anion radicals, and is covered with a singlet oxygen, electron

transfer, and the complex of the non-radical ways, which jointly promote the efficient degradation of pollutants.

For reactions involving both the radical pathway and the non-radical pathway, researchers have done many experiments to demonstrate the existence of active species (including quenching experiments, EPR experiments, electrochemical experiments, etc.). For instance, Fu et al. [59] synthesized a Fe_3O_4 -graphitized porous biological carbon composite catalyst ($\text{Fe}_3\text{O}_4/\text{MC}$) to activate PMS to degrade *p*-hydroxybenzoic acid. In the quenching experiment, phenol, NB, and BQ can inhibit HBA degradation, proving that $\text{SO}_4^{\cdot-}$, $\cdot\text{OH}$ and $\text{O}_2^{\cdot-}$ are involved in the reaction, and mainly induced by $\text{SO}_4^{\cdot-}$ and $\cdot\text{OH}$. The presence of NaClO_4 also inhibited the removal of HBA, and combined with EIS and LSV, it was proven that there was a non-radical pathway supplemented by electron transfer pathway in the system. The combination of radical and non-radical pathway promotes the degradation of pollutants. Miao et al. [91] synthesized a Fe and N co-doped carbon-based catalyst (FeCN_x) to activate PMS, and explored the mechanism of this system in the degradation of BPA. The presence of $^1\text{O}_2$ and surface-bound $\text{SO}_4^{\cdot-}$ and $\cdot\text{OH}$ was confirmed by the quenching experiment and EPR detection. In addition, FeCN_x and the PMS adsorbed on the surface of the catalyst and formed a stable and highly active complex (catalyst-PMS*). The electron transfer from BPA to catalyst-PMS* was mediated by the catalyst, triggering the formation of the complex and promoting the degradation of BPA (Figure 5). Dung et al. [92] synthesized a $\text{Fe}_3\text{O}_4/\text{CoCO}_3/\text{rGO}$ magnetic catalyst by a one-step solvothermal method to activate PMS and degrade rhodamine dye. Both $\text{SO}_4^{\cdot-}$ and $^1\text{O}_2$ contribute greatly to the degradation of rhodamine by the radical and non-radical pathways. In addition, the combination of these two ways also has a good removal effect for other dyes, reflecting the width of its application.

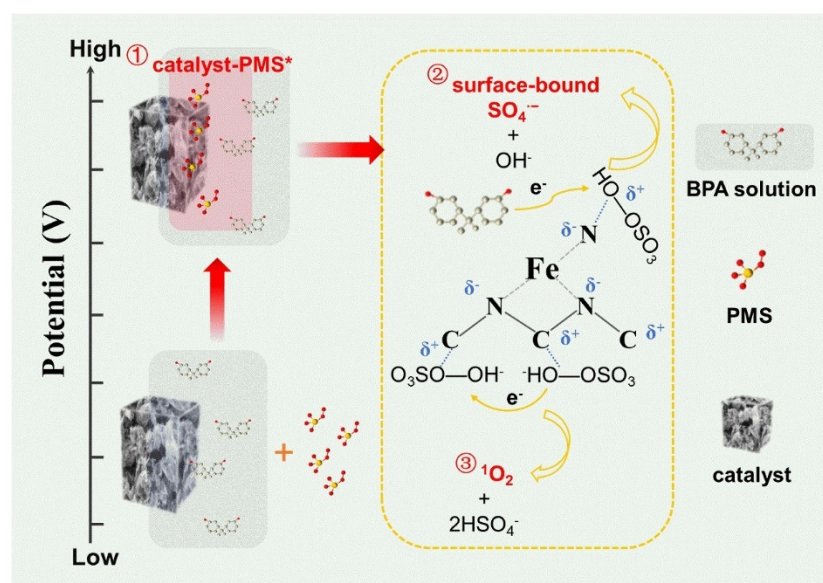


Figure 5. Mechanism of removal of BPA by FeCN_x/PMS system [91].

The synergistic effect of the radical and non-free radical pathways can effectively promote the degradation of pollutants, especially some structurally stable pollutants (such as phenolic substances). The above studies indicate that the combination of the radical and non-radical pathways can extend the application range of the system, and it has a good application prospect for the treatment of practical wastewater with complex components.

4. The Application of the Persulfate/Magnetic Catalyst System

Due to the rapid development of industry and agriculture, refractory organic pollutants not only exist in wastewater, but also in landfill leachate, biological waste sludge, and

soil. A persulfate/magnetic catalyst system has some applications in these practical fields (Table 3), and some specific cases are described in the following sections.

Table 3. The application of persulfate/magnetic catalyst system in actual wastewater, landfill leachate, biological waste, sludge, and soil.

Practical Field	Reaction System	Reaction Conditions	Results	Refs.
Actual wastewater	PVP-NZVI-Cu/PDS	[PDS] = 18 mmol/L; [catalyst] = 1.2 g/L; [TCE] = 0.15 mmol/L; pH = 3.2; t = 1 h	99.5% of TCE removal	[103]
	Mag-CuO/PMS	[Na ₂ SO ₄] = 0.2 mol/L; [PMS] = 2 mmol/L; [catalyst] = 0.1 g/L; pH = 7; t = 30 min; [AO7] = 0.2 mmol/L, [MB] = [RhB] = [ATZ] = 0.1 mmol/L	The removal efficiencies of AO7, MB, RhB, and ATZ were 95.81%, 74.57%, 100%, and 100%, respectively.	[104]
Landfill leachate	ZVINFS/rULGO/PDS	[PDS/COD] = 3; [catalyst] = 1.6 g/L; pH = 3; t = 45 min	80.87% removal of COD and 72.38% of NH ₃ removal	[105]
	CuFe ₂ O ₄ /PDS	[PDS] = 5 g/L; [catalyst] = 1.5 g/L; pH = 2; t = 60 min	57% removal of COD, 71% removal of NH ₃ -N and 63% of color, respectively.	[106]
	Fe ₂ O ₃ /Co ₃ O ₄ /EG/PDS	[PDS] = 0.05 mol/L; [catalyst] = 0.1 g; pH = 5; t = 60 min	90.6% removal of COD and 67.1% of NH ₄ ⁺ -N removal	[107]
Biological waste sludge	ZVI/PMS	[PMS] = 24.5 mg/g TSS; [catalyst] = 260.7 mg/g TSS	SRF decreased by 83.6%	[108]
	UV/ZVI/PDS	[n _{ZVI/PDS}] = 0.6; [PDS] = 200 mg/g TSS; UV = 254 nm; pH = 6.54; t = 20 min	64.0% decreased of CST and 78.2% decreased of SRF	[109]
	VTM/RH/PMS	[PMS] = 200 mg/g TSS; [VTM] = 1 g/g TSS; [RH] = 200 mg/g TSS	94.8% reduction of CST and 63.4% of Wc	[110]
Soil	Fe@CF-N/PMS	[PMS] = 0.2 mmol/L; [catalyst] = 25 mg; pH = 5; t = 180 min; [FLT] = 10 mg/L	78.12% removal of FLT	[111]
	Fe-Cu@BC-GM/PMS	[PMS] = 100 mg/L; [catalyst] = 100 mg/L; pH = 3; t = 120 min; [NAP] = 10 mg/L	67.98% removal of NAP	[112]
	nZVI/PDS	[n _{SMX/PDS}] = 1/75; [catalyst] = 0.03 g/g soil; [soil/water] = 1/1	Removal efficiencies of SMX were 87.6% (cinnamon soil), 90.6% (yellow brown earths), 80.8% (brown earths), 86.5% (black soils), and 96.1% (red earths), respectively.	[113]

4.1. Actual Wastewater

The actual wastewater is complex and has a certain buffer capacity. In the treatment of real wastewater, some researchers have made some good progress by activating persulfate systems with magnetic materials. For example, Adrees et al. [103] synthesized polyvinylpyrrolidone coated Fe-Cu nanomagnetic particles (PVP-nZVI-Cu) to activate PDS to remove trichloroethylene (TCE) from groundwater, and PVP effectively prevents the agglomeration of Fe-Cu nanoparticles. However, when the catalyst dosage is 1.2 g/L and the oxidant dosage is 18 mM, the TCE removal effect of the PVP-nZVI-Cu/PDS system can reach 99.5% within 60 min, and the dechlorination rate and mineralization rate can also

reach 81.1% and 83.8%, respectively. In the system, sulfate radicals and hydroxyl radicals play a major role, whereas superoxide anion radicals play a secondary role. Overall, the system has great potential for remediation of TCE contaminated groundwater. Li et al. [104] synthesized a magnetic copper oxide catalyst (Mag-CuO) by a simple one-step precipitation method, which was used to activate PMS to treat organic pollutants in wastewater containing high salinity. In a 0.2 mol/L sodium sulfate wastewater system, the Mag-CuO/PMS system can effectively remove acid orange 7 (95.81%), methylene blue (74.57%), rhodamine B (100%), and atrazine (100%), and still maintain good catalytic activity in the system with multiple salt components. In addition, studies have shown that a singlet oxygen is the main active species in the system due to the redox cycle of Cu and Fe ($\text{Fe}^{2+}/\text{Fe}^{3+}$ and $\text{Cu}^+/\text{Cu}^{2+}$) and the hydroxylation of the material surface, because singlet oxygen is less affected by the background components in the wastewater than other radicals. At present, although magnetic materials activated by a persulfate system in the laboratory model of wastewater have made a lot of excellent progress in the study, the actual wastewater composition is complicated, so more studies that are more biased towards actual wastewater are needed.

4.2. Landfill Leachate

Landfill leachate is produced by rainwater or groundwater infiltration into the landfill site during the solid waste landfill process, and it has the characteristics of toxicity and low biodegradability [114]. Landfill leachate could pollute soil and groundwater because of improper treatment, which can cause potential harm to human beings and ecological environments [115]. Soubh et al. [105] used chemically expanded GO as a carrier, prepared nanofiber/super-large reduced graphene composite (ZVINFS/rULGO) by reducing Fe^{2+} to ZVI supported on GO under the action of reducing agent sodium borohydride, which was used to treat landfill leachate in persulfate systems. On the one hand, the ZVINFS/rULGO/PDS system reduced the activation energy of COD and NH_3 by 3.8 times and 4.2 times, respectively, which was conducive to the removal of COD and NH_3 . On the other hand, the BOD_5/COD of landfill leachate increased from 0.25 to 0.52, which improved the biodegradability of landfill leachate. Karimipourfard et al. [106] synthesized CuFe_2O_4 magnetic material for persulfate activation to treat municipal garbage leachate by a simple ultrasonic coprecipitation method. Under the strong oxidation capacity of sulfate radicals, the removal rates of COD, $\text{NH}_3\text{-N}$, and chroma in landfill leachate by $\text{CuFe}_2\text{O}_4/\text{PDS}$ system are 57%, 71%, and 63%, respectively. Furthermore, Karimipourfard et al. [116] also investigated the preparation of $\text{CuFe}_2\text{O}_4/\text{rGO}$ composites by loading CuFe_2O_4 onto reduced graphene. As the graphene carrier provides a larger specific surface area and higher catalytic activity for the oxidation reaction, compared with the $\text{CuFe}_2\text{O}_4/\text{PDS}$ system under the optimal conditions, the removal of COD and $\text{NH}_3\text{-N}$ by $\text{CuFe}_2\text{O}_4/\text{RGO}/\text{PDS}$ system is further improved by 18.4% and 19.6%, respectively. Guo et al. [107] synthesized a peeled-graphite fixed ferrous oxide/cobalt oxide composite magnetic catalyst ($\text{Fe}_2\text{O}_3/\text{Co}_3\text{O}_4/\text{EG}$) by a heating-precipitation method, which was used to activate potassium persulfate to treat landfill leachate. Under optimal conditions, the removal of COD and $\text{NH}_4^+\text{-N}$ reached 67.1% and 90.6%, respectively. In general, all the catalysts mentioned above have good recovery performance and reuse performance in the treatment of landfill leachate, which also confirms that PDS activation by a magnetic catalyst has a good application prospect in the treatment of landfill leachate.

4.3. Biological Waste Sludge

Biological waste sludge is a by-product of biological wastewater treatment, with a high moisture content. Its subsequent treatment causes significant economic and environmental burden, and improper treatment of sludge is easy to cause secondary pollution, which poses potential threats to human health and ecological environments [117,118]. Pre-treatment of biological waste sludge and reduction of its moisture content can effectively reduce the volume of sludge and reduce its transportation and disposal costs [119]. The studies showed that the spatial distribution of extracellular polymeric substances (EPS) affects the

sedimentation, biological flocculation, and dehydration performance of sludge [120,121]. Therefore, by changing the affinity of EPS to water molecules and improving the filtration capacity of sludge (i.e., reducing the specific filtration resistance (SRF) of sludge), the dehydration performance of sludge can be effectively improved, making it easy to store, transport, and treat [118]. Li et al. [108] used ZVI to activate persulfate to improve the dehydration capacity of sludge by reducing the specific filtration resistance of sludge. Under the heat assisted treatment at 50 °C, ZVI activates persulfate to produce sulfate radicals and hydroxyl radicals. Heat treatment accelerates the production of radicals and the redox process, and effectively improves the dehydration capacity of sludge (the reduction rate of SRF of biological waste sludge is 90.6%). Zhang et al. [109] pointed out that with the help of ultraviolet light, PDS activated by ZVI can also effectively degrade extracellular polymer, reducing the SRF of biological waste sludge by 78.2%. Positive ions such as Fe^{2+} , Fe^{3+} , and H^+ in the system can reduce the electronegativity of sludge surface and promote the agglomeration of sludge particles, thus improving the dewatering performance of sludge. In Liu's study, rice husk (RH) was used as the skeleton construction agent for the first time to activate PMS with natural (VTM) to improve the dehydration performance of biological waste sludge (VTM-PMS-RH) [110]. Under the optimal conditions, capillary suction time (CST) reduction and water content of sludge cake (Wc) were 94.8% and 63.4%, respectively. In addition, heavy metals (Cu, Zn, Cr and Pb) in waste sludge are transformed into more stable forms, reducing their leaching toxicity and thus reducing environmental risks. Yang et al. [122] used a combination of manganese ferrite/biochar (MFB)-activated PMS and tannic acid (TA) to improve the dewatering performance of biological waste sludge. The addition of TA can promote the valence state conversion of iron and manganese ($\text{Fe}^{2+}/\text{Fe}^{3+}$ and $\text{Mn}^{2+}/\text{Mn}^{3+}$), accelerate the activation of PMS, produce species with strong oxidation activity, and improve the redox capacity of the system. In addition, it is worth noting that the dehydrated sludge treated by MFB/PMS/TA is not only conducive to incineration that can generate more energy, but also can be used as a precursor system to prepare biochar with well-developed pore structure, which has a good prospect of resource utilization and is a promising and effective way to treat biological waste sludge. In general, a magnetic catalyst-activated persulfate system can effectively improve the dewatering performance of waste sludge, and has a good application status and prospects in the treatment of biological waste sludge.

4.4. Soil

With the development of industry and agriculture, the massive discharge of waste water and waste gas not only enters into the water, but also enters into the soil, and the existence of persistent refractory organic pollutants causes serious soil pollution [123]. Since the soil environment has limited ability to repair itself, it is very important to find effective methods to degrade organic pollutants in soil [111]. For example, Li et al. [111] prepared N-doped carbon foam-loaded Fe nanoparticle composites (Fe@CF-N) by an in-situ impregnation and unique roasting method for activating PMS to degrade fluoranthene (FLT) in soil. Fe@CF-N has a large specific surface area ($249 \text{ m}^2 \cdot \text{g}^{-1}$), which can provide more adsorption sites and active sites for the reaction. Within 180 min, the removal of FLT reached 78.12%, and sulfate radicals, hydroxyl radicals, and singlet oxygen are all involved in the degradation of FLT. Finally, the results of plant toxicity test showed that seed germination rate and root cap elongation of Fe@CF-N/PMS-treated soil were not significantly different from that of uncontaminated soil, which proved that Fe@CF-N/PMS system can be well used to treat contaminated soil. Similarly, Zhu et al. [112] synthesized Fe/Cu nanoparticle composite catalysts (Fe-Cu@BC-GM) supported by biochar/geopolymer by an impregnation-roasting method to activate PMS for remediation of soil contaminated with naphthalene (NAP). The synergistic effect between Fe and Cu (redox pair between $\text{Fe}^{2+}/\text{Fe}^{3+}$ and $\text{Cu}^+/\text{Cu}^{2+}$) effectively promoted the decomposition of PMS to produce sulfate radicals and hydroxyl radicals, which were used to degrade NAP. Moreover, the plant toxicity test also showed that the germination rate, root cap elongation, and diameter length of mung bean seeds

in the soil treated by Fe-Cu@BC-GM/PMS system were not significantly different from that of unpolluted soil, which also can prove that the persulfate/magnetic catalyst system can be used to treat contaminated soil. Zhou et al. [113] used ZVI nanoparticles to activate PDS to rehabilitate sulfamethoxazole (SMX) contaminated agricultural soils (cinnamon). Due to the weak alkalinity of the system (pH = 8.5), the active species generated during the reaction were mainly hydroxyl radicals, and the removal rate of SMX was 87.6% within 4 h. The removal rate of SMX in different types of agricultural soil (such as yellow brown soil, brown soil, black soil, and red soil) by the nZVI/PDS system is above 80%, indicating that the system has a certain positive effect on the removal of pollutants in agricultural soil. The application of magnetic catalyst-activated persulfate system in soil is still few and needs further experimental exploration.

5. Challenges and Perspectives

The magnetic catalyst activation of the persulfate system in wastewater containing refractory organic pollutants has achieved many good results, but there are still some limitations, and in this regard, here are some prospects to put forward:

- (1) According to the magnetic species, magnetic catalysts can be roughly divided into iron-based catalyst, cobalt-based catalyst, nickel-based catalyst, and supported magnetic catalyst, and the most common is the magnetic carbon composite catalyst. However, the magnetic catalyst/persulfate system is still in the development stage and is rarely used in actual wastewater. The actual wastewater composition is complex, and in future research, we can design catalyst materials with better performance or optimize existing materials to cope with the complex composition and environment of the actual wastewater.
- (2) The reaction mechanism of magnetic catalyst activation of persulfate includes the radical pathway and the non-radical pathway, which is related to the nature of the catalyst. However, some studies are not comprehensive enough for the radicals trapping experiments and EPR/ESR experiments involved in the reaction system, which may lead to a lack of comprehensive understanding of the reaction mechanism. In future research, we can combine representational means and experimental means to carry out more in-depth and comprehensive research and summary.
- (3) A variety of magnetic catalysts can be used to treat refractory organic pollutants in the aqueous phase, including phenols, antibiotics, dyes, chlorinated organic pollutants, etc., but these are in the research stage of laboratory model wastewater, and there are few cases of actual wastewater treatment. In future research, the magnetic catalyst and magnetic catalyst/persulfate technology can be optimized and perfected. It is necessary to consider the switch from the laboratory scale to the middle scale, and apply the magnetic catalyst-activated persulfate system with high efficiency and low energy consumption, and make recovery of the treatment of refractory organic pollutants easy in the actual environment as soon as possible.

6. Summary and Outlook

In this paper, the activation mechanism of persulfate by different magnetic catalysts is introduced, including an iron-based catalyst, cobalt-based catalyst, nickel-based catalyst, and supported magnetic catalyst. The activation of persulfate by these magnetic catalysts generally involves the radical pathway and the non-radical pathway. Two methods of identifying active species involved in these two pathways (quench experiment and EPR/ESR experiment) are summarized, and the electrochemical reactions involved in electron transfer and complex formation in the non-radical pathway are also illustrated, respectively. Finally, we also list the cases in practical application. At present, there are increasing successful cases, but its practical application scope is not broad enough. In general, a magnetic catalyst has a good application prospect, which needs to be explored in the future experiments. Our aim is to make full use of a magnetic catalyst that has low energy consumption and high

efficiency, and is easy to recycle and reuse, so that a magnetic catalyst/persulfate system can be put into practical environmental treatment as soon as possible.

Author Contributions: K.T.: Writing—Original Draft Preparation; F.S.: Writing—Review and Editing; M.C.: Writing—Review and Editing; Q.Z.: Conceptualization; G.Z.: Conceptualization, Writing—Review and Editing, Supervision, and Funding acquisition. All authors have read and agreed to the published version of the manuscript.

Funding: The work was supported by the Open Project of State Key Laboratory of Urban Water Resource and Environment, Harbin Institute of Technology (ES202206), and Talents of High Level Scientific Research Foundation of Qingdao Agricultural University (6651120004) for their financial support.

Conflicts of Interest: The authors declare no conflict of interest.

References

1. Gosset, A.; Ferro, Y.; Durrieu, C. Methods for evaluating the pollution impact of urban wet weather discharges on biocenosis: A review. *Water Res.* **2016**, *89*, 330–354. [[CrossRef](#)] [[PubMed](#)]
2. Waclawek, S.; Lutze, H.V.; Grübel, K.; Padil, V.V.T.; Černík, M.; Dionysiou, D.D. Chemistry of persulfates in water and wastewater treatment: A review. *Chem. Eng. J.* **2017**, *330*, 44–62. [[CrossRef](#)]
3. Huang, D.; Sun, X.; Liu, Y.; Ji, H.; Liu, W.; Wang, C.-C.; Ma, W.; Cai, Z. A carbon-rich g-C₃N₄ with promoted charge separation for highly efficient photocatalytic degradation of amoxicillin. *Chin. Chem. Lett.* **2021**, *32*, 2787–2791. [[CrossRef](#)]
4. Wang, H.; Zhang, J.; Wang, P.; Yin, L.; Tian, Y.; Li, J. Bifunctional copper modified graphitic carbon nitride catalysts for efficient tetracycline removal: Synergy of adsorption and photocatalytic degradation. *Chin. Chem. Lett.* **2020**, *31*, 2789–2794. [[CrossRef](#)]
5. Ozyildiz, G.; Olmez-Hanci, T.; Arslan-Alaton, I. Effect of nano-scale, reduced graphene oxide on the degradation of bisphenol A in real tertiary treated wastewater with the persulfate/UV-C process. *Appl. Catal. B-Environ.* **2019**, *254*, 135–144. [[CrossRef](#)]
6. Li, J.; Ren, Y.; Ji, F.; Lai, B. Heterogeneous catalytic oxidation for the degradation of *p*-nitrophenol in aqueous solution by persulfate activated with CuFe₂O₄ magnetic nano-particles. *Chem. Eng. J.* **2017**, *324*, 63–73. [[CrossRef](#)]
7. Tian, K.; Hu, L.; Li, L.; Zheng, Q.; Xin, Y.; Zhang, G. Recent advances in persulfate-based advanced oxidation processes for organic wastewater treatment. *Chin. Chem. Lett.* **2022**, *33*, 4461–4477. [[CrossRef](#)]
8. Qu, J.H.; Tian, X.; Zhang, X.B.; Yao, J.Y.; Xue, J.Q.; Li, K.G.; Zhang, B.; Wang, L.; Zhang, Y. Free radicals-triggered reductive and oxidative degradation of highly chlorinated compounds via regulation of heat-activated persulfate by low-molecular-weight organic acids. *Appl. Catal. B-Environ.* **2022**, *310*, 121359. [[CrossRef](#)]
9. Qu, J.H.; Xu, Y.; Zhang, X.B.; Sun, M.Z.; Tao, Y.; Zhang, X.M.; Zhang, G.S.; Ge, C.J.; Zhang, Y. Ball milling-assisted preparation of N-doped biochar loaded with ferrous sulfide as persulfate activator for phenol degradation: Multiple active sites-triggered radical/non-radical mechanism. *Appl. Catal. B-Environ.* **2022**, *316*, 121639. [[CrossRef](#)]
10. Ike, I.A.; Linden, K.G.; Orbell, J.D.; Duke, M. Critical review of the science and sustainability of persulphate advanced oxidation processes. *Chem. Eng. J.* **2018**, *338*, 651–669. [[CrossRef](#)]
11. Tran, N.H.; Reinhard, M.; Gin, K.Y. Occurrence and fate of emerging contaminants in municipal wastewater treatment plants from different geographical regions—a review. *Water Res.* **2018**, *133*, 182–207. [[CrossRef](#)] [[PubMed](#)]
12. Yang, C.; Wang, P.; Li, J.; Wang, Q.; Xu, P.; You, S.; Zheng, Q.; Zhang, G. Photocatalytic PVDF ultrafiltration membrane blended with visible-light responsive Fe(III)-TiO₂ catalyst: Degradation kinetics, catalytic performance and reusability. *Chem. Eng. J.* **2021**, *417*, 129340. [[CrossRef](#)]
13. Duan, X.; Sun, H.; Wang, S. Metal-Free Carbocatalysis in Advanced Oxidation Reactions. *Acc. Chem. Res.* **2018**, *51*, 678–687. [[CrossRef](#)] [[PubMed](#)]
14. Tufail, A.; Price, W.E.; Mohseni, M.; Pramanik, B.K.; Hai, F.I. A critical review of advanced oxidation processes for emerging trace organic contaminant degradation: Mechanisms, factors, degradation products, and effluent toxicity. *J. Water Process Eng.* **2021**, *40*, 101778. [[CrossRef](#)]
15. Bennajah, M.; Elkacmi, R. Advanced oxidation technologies for the treatment and detoxification of olive mill wastewater: A general review. *J. Water Reuse Desalin.* **2019**, *9*, 463–505. [[CrossRef](#)]
16. Ganiyu, S.O.; Martínez-Huitle, C.A.; Oturan, M.A. Electrochemical advanced oxidation processes for wastewater treatment: Advances in formation and detection of reactive species and mechanisms. *Curr. Opin. Electrochem.* **2021**, *27*, 100678. [[CrossRef](#)]
17. Yang, J.; Liu, X.; Wang, D.; Xu, Q.; Yang, Q.; Zeng, G.; Li, X.; Liu, Y.; Gong, J.; Ye, J.; et al. Mechanisms of peroxymonosulfate pretreatment enhancing production of short-chain fatty acids from waste activated sludge. *Water Res.* **2019**, *148*, 239–249. [[CrossRef](#)]
18. Moreira, F.C.; Boaventura, R.A.R.; Brillas, E.; Vilar, V.J.P. Electrochemical advanced oxidation processes: A review on their application to synthetic and real wastewaters. *Appl. Catal. B-Environ.* **2017**, *202*, 217–261. [[CrossRef](#)]
19. Neyens, E. Advanced sludge treatment affects extracellular polymeric substances to improve activated sludge dewatering. *J. Hazard. Mater.* **2004**, *106*, 83–92. [[CrossRef](#)]

20. Xiao, S.; Cheng, M.; Zhong, H.; Liu, Z.; Liu, Y.; Yang, X.; Liang, Q. Iron-mediated activation of persulfate and peroxymonosulfate in both homogeneous and heterogeneous ways: A review. *Chem. Eng. J.* **2020**, *384*, 123265. [[CrossRef](#)]
21. Wang, J.; Liao, Z.; Ifthikar, J.; Shi, L.; Du, Y.; Zhu, J.; Xi, S.; Chen, Z.; Chen, Z. Treatment of refractory contaminants by sludge-derived biochar/persulfate system via both adsorption and advanced oxidation process. *Chemosphere* **2017**, *185*, 754–763. [[CrossRef](#)] [[PubMed](#)]
22. Fan, J.; Gu, L.; Wu, D.; Liu, Z. Mackinawite (FeS) activation of persulfate for the degradation of *p*-chloroaniline: Surface reaction mechanism and sulfur-mediated cycling of iron species. *Chem. Eng. J.* **2018**, *333*, 657–664. [[CrossRef](#)]
23. Zhu, L.; Ai, Z.; Ho, W.; Zhang, L. Core-shell Fe-Fe₂O₃ nanostructures as effective persulfate activator for degradation of methyl orange. *Sep. Purif. Technol.* **2013**, *108*, 159–165. [[CrossRef](#)]
24. Zhang, B.-T.; Zhang, Y.; Teng, Y.; Fan, M. Sulfate Radical and Its Application in Decontamination Technologies. *Crit. Rev. Environ. Sci. Technol.* **2014**, *45*, 1756–1800. [[CrossRef](#)]
25. Karim, A.V.; Jiao, Y.; Zhou, M.; Nidheesh, P.V. Iron-based persulfate activation process for environmental decontamination in water and soil. *Chemosphere* **2021**, *265*, 129057. [[CrossRef](#)] [[PubMed](#)]
26. Duan, X.; Yang, S.; Waclawek, S.; Fang, G.; Xiao, R.; Dionysiou, D.D. Limitations and prospects of sulfate-radical based advanced oxidation processes. *J. Environ. Chem. Eng.* **2020**, *8*, 103849. [[CrossRef](#)]
27. Rastogi, A.; Al-Abed, S.R.; Dionysiou, D.D. Sulfate radical-based ferrous-peroxymonosulfate oxidative system for PCBs degradation in aqueous and sediment systems. *Appl. Catal. B-Environ.* **2009**, *85*, 171–179. [[CrossRef](#)]
28. Li, C.-X.; Chen, C.-B.; Lu, J.-Y.; Cui, S.; Li, J.; Liu, H.-Q.; Li, W.-W.; Zhang, F. Metal organic framework-derived CoMn₂O₄ catalyst for heterogeneous activation of peroxymonosulfate and sulfanilamide degradation. *Chem. Eng. J.* **2018**, *337*, 101–109. [[CrossRef](#)]
29. Wang, F.; Wu, C.; Li, Q. Treatment of refractory organics in strongly alkaline dinitrodiazophenol wastewater with microwave irradiation-activated persulfate. *Chemosphere* **2020**, *254*, 126773. [[CrossRef](#)]
30. Mahdi-Ahmed, M.; Chiron, S. Ciprofloxacin oxidation by UV-C activated peroxymonosulfate in wastewater. *J. Hazard. Mater.* **2014**, *265*, 41–46. [[CrossRef](#)]
31. Fedorov, K.; Plata-Gryl, M.; Khan, J.A.; Boczkaj, G. Ultrasound-assisted heterogeneous activation of persulfate and peroxymonosulfate by asphaltenes for the degradation of BTEX in water. *J. Hazard. Mater.* **2020**, *397*, 122804. [[CrossRef](#)] [[PubMed](#)]
32. Qu, J.; Shi, J.; Wang, Y.; Tong, H.; Zhu, Y.; Xu, L.; Wang, Y.; Zhang, B.; Tao, Y.; Dai, X.; et al. Applications of functionalized magnetic biochar in environmental remediation: A review. *J. Hazard. Mater.* **2022**, *434*, 128841. [[CrossRef](#)]
33. Yin, F.; Wang, C.; Lin, K.-Y.A.; Tong, S. Persulfate activation for efficient degradation of norfloxacin by a rGO-Fe₃O₄ composite. *J. Taiwan Inst. Chem. Eng.* **2019**, *102*, 163–169. [[CrossRef](#)]
34. Hu, L.; Wang, P.; Liu, G.; Zheng, Q.; Zhang, G. Catalytic degradation of *p*-nitrophenol by magnetically recoverable Fe₃O₄ as a persulfate activator under microwave irradiation. *Chemosphere* **2020**, *240*, 124977. [[CrossRef](#)] [[PubMed](#)]
35. Cui, X.; Zhang, S.-S.; Geng, Y.; Zhen, J.; Zhan, J.; Cao, C.; Ni, S.-Q. Synergistic catalysis by Fe₃O₄-biochar/persulfate system for the removal of bisphenol a. *Sep. Purif. Technol.* **2021**, *276*, 119351. [[CrossRef](#)]
36. Rodriguez, S.; Santos, A.; Romero, A. Oxidation of priority and emerging pollutants with persulfate activated by iron: Effect of iron valence and particle size. *Chem. Eng. J.* **2017**, *318*, 197–205. [[CrossRef](#)]
37. Wu, J.; Wang, B.; Blaney, L.; Peng, G.; Chen, P.; Cui, Y.; Deng, S.; Wang, Y.; Huang, J.; Yu, G. Degradation of sulfamethazine by persulfate activated with organo-montmorillonite supported nano-zero valent iron. *Chem. Eng. J.* **2019**, *361*, 99–108. [[CrossRef](#)]
38. Zhang, Y.; Xu, X.; Pan, Y.; Xu, L.; Zhou, M. Pre-magnetized Fe⁰ activated persulfate for the degradation of nitrobenzene in groundwater. *Sep. Purif. Technol.* **2019**, *212*, 555–562. [[CrossRef](#)]
39. Zhen, G.; Lu, X.; Su, L.; Kobayashi, T.; Kumar, G.; Zhou, T.; Xu, K.; Li, Y.Y.; Zhu, X.; Zhao, Y. Unraveling the catalyzing behaviors of different iron species (Fe(2+) vs. Fe(0)) in activating persulfate-based oxidation process with implications to waste activated sludge dewaterability. *Water Res.* **2018**, *134*, 101–114. [[CrossRef](#)]
40. Hou, K.; Pi, Z.; Yao, F.; Wu, B.; He, L.; Li, X.; Wang, D.; Dong, H.; Yang, Q. A critical review on the mechanisms of persulfate activation by iron-based materials: Clarifying some ambiguity and controversies. *Chem. Eng. J.* **2021**, *407*, 127078. [[CrossRef](#)]
41. Palharim, P.H.; Graca, C.A.L.; Teixeira, A. Comparison between UVA- and zero-valent iron-activated persulfate processes for degrading propylparaben. *Environ. Sci. Pollut. Res. Int.* **2020**, *27*, 22214–22224. [[CrossRef](#)] [[PubMed](#)]
42. Hayat, W.; Zhang, Y.; Hussain, I.; Du, X.; Du, M.; Yao, C.; Huang, S.; Si, F. Efficient degradation of imidacloprid in water through iron activated sodium persulfate. *Chem. Eng. J.* **2019**, *370*, 1169–1180. [[CrossRef](#)]
43. El Fakir, A.A.; Anfar, Z.; Amedlous, A.; Amjlef, A.; Farsad, S.; Jada, A.; El Alem, N. Synergistic effect for efficient catalytic persulfate activation in conducting polymers-hematite sand composites: Enhancement of chemical stability. *Appl. Catal. A-Gen.* **2021**, *623*, 118246. [[CrossRef](#)]
44. Yang, M.; Ren, X.; Hu, L.; Guo, W.; Zhan, J. Facet-controlled activation of persulfate by goethite for tetracycline degradation in aqueous solution. *Chem. Eng. J.* **2021**, *412*, 128628. [[CrossRef](#)]
45. Lv, J.; Gong, L.; Chen, X.; Liu, B.; Li, Y.; Jiang, J.; Zhou, J. Enhancements of short-chain fatty acids production via anaerobic fermentation of waste activated sludge by the combined use of persulfate and micron-sized magnetite. *Bioresour. Technol.* **2021**, *342*, 126051. [[CrossRef](#)] [[PubMed](#)]
46. Sun, S.; Ren, J.; Liu, J.; Rong, L.; Wang, H.; Xiao, Y.; Sun, F.; Mei, R.; Chen, C.; Su, X. Pyrite-activated persulfate oxidation and biological denitrification for effluent of biological landfill leachate treatment system. *J. Environ. Manag.* **2022**, *304*, 114290. [[CrossRef](#)]

47. Zhao, Y.S.; Sun, C.; Sun, J.Q.; Zhou, R. Kinetic modeling and efficiency of sulfate radical-based oxidation to remove p-nitroaniline from wastewater by persulfate/Fe₃O₄ nanoparticles process. *Sep. Purif. Technol.* **2015**, *142*, 182–188. [[CrossRef](#)]
48. Yan, J.; Lei, M.; Zhu, L.; Anjum, M.N.; Zou, J.; Tang, H. Degradation of sulfamonomethoxine with Fe₃O₄ magnetic nanoparticles as heterogeneous activator of persulfate. *J. Hazard. Mater.* **2011**, *186*, 1398–1404. [[CrossRef](#)]
49. Hussain, I.; Zhang, Y.; Li, M.; Huang, S.; Hayat, W.; He, L.; Du, X.; Liu, G.; Du, M. Heterogeneously degradation of aniline in aqueous solution using persulfate catalyzed by magnetic BiFeO₃ nanoparticles. *Catal. Today* **2018**, *310*, 130–140. [[CrossRef](#)]
50. Guan, Y.H.; Ma, J.; Ren, Y.M.; Liu, Y.L.; Xiao, J.Y.; Lin, L.Q.; Zhang, C. Efficient degradation of atrazine by magnetic porous copper ferrite catalyzed peroxymonosulfate oxidation via the formation of hydroxyl and sulfate radicals. *Water Res.* **2013**, *47*, 5431–5438. [[CrossRef](#)]
51. Tian, X.; Tian, C.; Nie, Y.; Dai, C.; Yang, C.; Tian, N.; Zhou, Z.; Li, Y.; Wang, Y. Controlled synthesis of dandelion-like NiCo₂O₄ microspheres and their catalytic performance for peroxymonosulfate activation in humic acid degradation. *Chem. Eng. J.* **2018**, *331*, 144–151. [[CrossRef](#)]
52. Wu, Z.; Liang, Y.; Zou, D.; Yuan, X.; Xiao, Z.; Deng, Y.; Zhou, Y.; Jiang, L.; Qin, P. Enhanced heterogeneous activation of persulfate by Ni_xCo_{3-x}O₄ for oxidative degradation of tetracycline and bisphenol A. *J. Environ. Chem. Eng.* **2020**, *8*, 104451. [[CrossRef](#)]
53. Hu, L.; Zhang, G.; Liu, M.; Wang, Q.; Dong, S.; Wang, P. Application of nickel foam-supported Co₃O₄-Bi₂O₃ as a heterogeneous catalyst for BPA removal by peroxymonosulfate activation. *Sci. Total Environ.* **2019**, *647*, 352–361. [[CrossRef](#)]
54. Zhou, X.; Zhu, Y.; Niu, Q.; Zeng, G.; Lai, C.; Liu, S.; Huang, D.; Qin, L.; Liu, X.; Li, B.; et al. New notion of biochar: A review on the mechanism of biochar applications in advanced oxidation processes. *Chem. Eng. J.* **2021**, *416*, 129027. [[CrossRef](#)]
55. Dong, Y.D.; Zhang, L.Q.; Zhou, P.; Liu, Y.; Lin, H.; Zhong, G.J.; Yao, G.; Li, Z.M.; Lai, B. Natural cellulose supported carbon nanotubes and Fe₃O₄ NPs as the efficient peroxydisulfate activator for the removal of bisphenol A: An enhanced non-radical oxidation process. *J. Hazard. Mater.* **2022**, *423*, 127054. [[CrossRef](#)] [[PubMed](#)]
56. Zhang, Y.; Zhang, B.T.; Teng, Y.; Zhao, J.; Sun, X. Heterogeneous activation of persulfate by carbon nanofiber supported Fe₃O₄@carbon composites for efficient ibuprofen degradation. *J. Hazard. Mater.* **2021**, *401*, 123428. [[CrossRef](#)]
57. Xu, P.; Wang, P.; Wang, Q.; Wei, R.; Li, Y.; Xin, Y.; Zheng, T.; Hu, L.; Wang, X.; Zhang, G. Facile synthesis of Ag₂O/ZnO/rGO heterojunction with enhanced photocatalytic activity under simulated solar light: Kinetics and mechanism. *J. Hazard. Mater.* **2021**, *403*, 124011. [[CrossRef](#)]
58. Peng, Y.; Azeem, M.; Li, R.; Xing, L.; Li, Y.; Zhang, Y.; Guo, Z.; Wang, Q.; Ngo, H.H.; Qu, G.; et al. Zirconium hydroxide nanoparticle encapsulated magnetic biochar composite derived from rice residue: Application for As(III) and As(V) polluted water purification. *J. Hazard. Mater.* **2022**, *423*, 127081. [[CrossRef](#)]
59. Fu, H.; Zhao, P.; Xu, S.; Cheng, G.; Li, Z.; Li, Y.; Li, K.; Ma, S. Fabrication of Fe₃O₄ and graphitized porous biochar composites for activating peroxymonosulfate to degrade p-hydroxybenzoic acid: Insights on the mechanism. *Chem. Eng. J.* **2019**, *375*, 121980. [[CrossRef](#)]
60. Xu, Y.; Ai, J.; Zhang, H. The mechanism of degradation of bisphenol A using the magnetically separable CuFe₂O₄/peroxymonosulfate heterogeneous oxidation process. *J. Hazard. Mater.* **2016**, *309*, 87–96. [[CrossRef](#)]
61. Huang, Z.; Bao, H.; Yao, Y.; Lu, W.; Chen, W. Novel green activation processes and mechanism of peroxymonosulfate based on supported cobalt phthalocyanine catalyst. *Appl. Catal. B-Environ.* **2014**, *154–155*, 36–43. [[CrossRef](#)]
62. Hu, L.; Zhang, G.; Liu, M.; Wang, Q.; Wang, P. Enhanced degradation of Bisphenol A (BPA) by peroxymonosulfate with Co₃O₄-Bi₂O₃ catalyst activation: Effects of pH, inorganic anions, and water matrix. *Chem. Eng. J.* **2018**, *338*, 300–310. [[CrossRef](#)]
63. Yin, R.; Guo, W.; Wang, H.; Du, J.; Zhou, X.; Wu, Q.; Zheng, H.; Chang, J.; Ren, N. Enhanced peroxymonosulfate activation for sulfamethazine degradation by ultrasound irradiation: Performances and mechanisms. *Chem. Eng. J.* **2018**, *335*, 145–153. [[CrossRef](#)]
64. Xie, P.; Ma, J.; Liu, W.; Zou, J.; Yue, S.; Li, X.; Wiesner, M.R.; Fang, J. Removal of 2-MIB and geosmin using UV/persulfate: Contributions of hydroxyl and sulfate radicals. *Water Res.* **2015**, *69*, 223–233. [[CrossRef](#)] [[PubMed](#)]
65. Moon, Y.; Jafry, A.T.; Kang, S.B.; Seo, J.Y.; Baek, K.Y.; Kim, E.J.; Pan, J.G.; Choi, J.Y.; Kim, H.J.; Lee, K.H.; et al. Organophosphorus hydrolase-poly-beta-cyclodextrin as a stable self-decontaminating bio-catalytic material for sorption and degradation of organophosphate pesticide. *J. Hazard. Mater.* **2019**, *365*, 261–269. [[CrossRef](#)]
66. Chen, C.; Ma, T.; Shang, Y.; Gao, B.; Jin, B.; Dan, H.; Li, Q.; Yue, Q.; Li, Y.; Wang, Y.; et al. In-situ pyrolysis of Enteromorpha as carbocatalyst for catalytic removal of organic contaminants: Considering the intrinsic N/Fe in Enteromorpha and non-radical reaction. *Appl. Catal. B-Environ.* **2019**, *250*, 382–395. [[CrossRef](#)]
67. Xu, L.; Wang, J. Magnetic nanoscaled Fe₃O₄/CeO₂ composite as an efficient Fenton-like heterogeneous catalyst for degradation of 4-chlorophenol. *Environ. Sci. Technol.* **2012**, *46*, 10145–10153. [[CrossRef](#)]
68. Chen, X.; Oh, W.-D.; Hu, Z.-T.; Sun, Y.-M.; Webster, R.D.; Li, S.-Z.; Lim, T.-T. Enhancing sulfacetamide degradation by peroxy-monosulfate activation with N-doped graphene produced through delicately-controlled nitrogen functionalization via tweaking thermal annealing processes. *Appl. Catal. B-Environ.* **2018**, *225*, 243–257. [[CrossRef](#)]
69. Oh, W.-D.; Lisak, G.; Webster, R.D.; Liang, Y.-N.; Veksha, A.; Giannis, A.; Moo, J.G.S.; Lim, J.-W.; Lim, T.-T. Insights into the thermolytic transformation of lignocellulosic biomass waste to redox-active carbocatalyst: Durability of surface active sites. *Appl. Catal. B-Environ.* **2018**, *233*, 120–129. [[CrossRef](#)]
70. Huang, Y.M.; Li, G.; Li, M.; Yin, J.; Meng, N.; Zhang, D.; Cao, X.Q.; Zhu, F.P.; Chen, M.; Li, L.; et al. Kelp-derived N-doped biochar activated peroxymonosulfate for ofloxacin degradation. *Sci. Total Environ.* **2021**, *754*, 141999. [[CrossRef](#)]

71. Wang, Y.; Cao, D.; Zhao, X. Heterogeneous degradation of refractory pollutants by peroxymonosulfate activated by CoOx-doped ordered mesoporous carbon. *Chem. Eng. J.* **2017**, *328*, 1112–1121. [[CrossRef](#)]
72. Li, G.; Cao, X.-q.; Meng, N.; Huang, Y.-m.; Wang, X.-d.; Gao, Y.-y.; Li, X.; Yang, T.-s.; Li, B.-l.; Zhang, Y.-z.; et al. Fe₃O₄ supported on water caltrop-derived biochar toward peroxymonosulfate activation for urea degradation: The key role of sulfate radical. *Chem. Eng. J.* **2022**, *433*, 133595. [[CrossRef](#)]
73. Cheng, X.; Guo, H.; Zhang, Y.; Wu, X.; Liu, Y. Non-photochemical production of singlet oxygen via activation of persulfate by carbon nanotubes. *Water Res.* **2017**, *113*, 80–88. [[CrossRef](#)]
74. Liu, S.; Lai, C.; Zhou, X.; Zhang, C.; Chen, L.; Yan, H.; Qin, L.; Huang, D.; Ye, H.; Chen, W.; et al. Peroxydisulfate activation by sulfur-doped ordered mesoporous carbon: Insight into the intrinsic relationship between defects and ¹O₂ generation. *Water Res.* **2022**, *221*, 118797. [[CrossRef](#)] [[PubMed](#)]
75. Zhu, S.; Huang, X.; Ma, F.; Wang, L.; Duan, X.; Wang, S. Catalytic Removal of Aqueous Contaminants on N-Doped Graphitic Biochars: Inherent Roles of Adsorption and Nonradical Mechanisms. *Environ. Sci. Technol.* **2018**, *52*, 8649–8658. [[CrossRef](#)] [[PubMed](#)]
76. Fu, H.; Ma, S.; Zhao, P.; Xu, S.; Zhan, S. Activation of peroxymonosulfate by graphitized hierarchical porous biochar and MnFe₂O₄ magnetic nanoarchitecture for organic pollutants degradation: Structure dependence and mechanism. *Chem. Eng. J.* **2019**, *360*, 157–170. [[CrossRef](#)]
77. Wang, L.; Lan, X.; Peng, W.; Wang, Z. Uncertainty and misinterpretation over identification, quantification and transformation of reactive species generated in catalytic oxidation processes: A review. *J. Hazard. Mater.* **2021**, *408*, 124436. [[CrossRef](#)]
78. Niu, L.; Zhang, G.; Xian, G.; Ren, Z.; Wei, T.; Li, Q.; Zhang, Y.; Zou, Z. Tetracycline degradation by persulfate activated with magnetic γ-Fe₂O₃/CeO₂ catalyst: Performance, activation mechanism and degradation pathway. *Sep. Purif. Technol.* **2021**, *259*, 118156. [[CrossRef](#)]
79. Li, X.; Jia, Y.; Zhou, M.; Su, X.; Sun, J. High-efficiency degradation of organic pollutants with Fe, N co-doped biochar catalysts via persulfate activation. *J. Hazard. Mater.* **2020**, *397*, 122764. [[CrossRef](#)]
80. Xu, X.; Qin, J.; Wei, Y.; Ye, S.; Shen, J.; Yao, Y.; Ding, B.; Shu, Y.; He, G.; Chen, H. Heterogeneous activation of persulfate by NiFe_{2-x}Co_xO₄-RGO for oxidative degradation of bisphenol A in water. *Chem. Eng. J.* **2019**, *365*, 259–269. [[CrossRef](#)]
81. Liu, D.; Li, M.; Li, X.; Ren, F.; Sun, P.; Zhou, L. Core-shell Zn/Co MOFs derived Co₃O₄/CNTs as an efficient magnetic heterogeneous catalyst for persulfate activation and oxytetracycline degradation. *Chem. Eng. J.* **2020**, *387*, 124008. [[CrossRef](#)]
82. Liu, B.; Song, W.; Zhang, W.; Zhang, X.; Pan, S.; Wu, H.; Sun, Y.; Xu, Y. Fe₃O₄@CNT as a high-effective and steady chainmail catalyst for tetracycline degradation with peroxydisulfate activation: Performance and mechanism. *Sep. Purif. Technol.* **2021**, *273*, 118705. [[CrossRef](#)]
83. Shao, F.; Wang, Y.; Mao, Y.; Shao, T.; Shang, J. Degradation of tetracycline in water by biochar supported nanosized iron activated persulfate. *Chemosphere* **2020**, *261*, 127844. [[CrossRef](#)] [[PubMed](#)]
84. Guan, R.; Yuan, X.; Wu, Z.; Jiang, L.; Zhang, J.; Li, Y.; Zeng, G.; Mo, D. Efficient degradation of tetracycline by heterogeneous cobalt oxide/cerium oxide composites mediated with persulfate. *Sep. Purif. Technol.* **2019**, *212*, 223–232. [[CrossRef](#)]
85. Ouyang, M.; Li, X.; Xu, Q.; Tao, Z.; Yao, F.; Huang, X.; Wu, Y.; Wang, D.; Yang, Q.; Chen, Z.; et al. Heterogeneous activation of persulfate by Ag doped BiFeO₃ composites for tetracycline degradation. *J. Colloid Interface Sci.* **2020**, *566*, 33–45. [[CrossRef](#)]
86. Liu, T.; Wu, K.; Wang, M.; Jing, C.; Chen, Y.; Yang, S.; Jin, P. Performance and mechanisms of sulfadiazine removal using persulfate activated by Fe₃O₄@CuO_x hollow spheres. *Chemosphere* **2021**, *262*, 127845. [[CrossRef](#)]
87. Zhou, R.; Lu, S.; Su, Y.; Li, T.; Ma, T.; Ren, H. Hierarchically fusiform CuO microstructures decorated with Fe₃O₄ nanoparticles as novel persulfate activators for 4-aminobenzenesulfonic acid degradation in aqueous solutions. *J. Alloys Compd.* **2020**, *815*, 152394. [[CrossRef](#)]
88. Kim, H.H.; Lee, D.; Choi, J.; Lee, H.; Seo, J.; Kim, T.; Lee, K.M.; Pham, A.L.; Lee, C. Nickel-Nickel oxide nanocomposite as a magnetically separable persulfate activator for the nonradical oxidation of organic contaminants. *J. Hazard. Mater.* **2020**, *388*, 121767. [[CrossRef](#)]
89. Jiang, Z.; Zhao, J.; Li, C.; Liao, Q.; Xiao, R.; Yang, W. Strong synergistic effect of Co₃O₄ encapsulated in nitrogen-doped carbon nanotubes on the nonradical-dominated persulfate activation. *Carbon* **2020**, *158*, 172–183. [[CrossRef](#)]
90. Wang, J.; Kou, L.; Zhao, L.; Duan, W. One-pot fabrication of sludge-derived magnetic Fe, N-codoped carbon catalysts for peroxymonosulfate-induced elimination of phenolic contaminants. *Chemosphere* **2020**, *248*, 126076. [[CrossRef](#)]
91. Miao, W.; Liu, Y.; Wang, D.; Du, N.; Ye, Z.; Hou, Y.; Mao, S.; Ostrikov, K. The role of Fe-N_x single-atom catalytic sites in peroxymonosulfate activation: Formation of surface-activated complex and non-radical pathways. *Chem. Eng. J.* **2021**, *423*, 130250. [[CrossRef](#)]
92. Dung, N.T.; Trang, T.T.; Thao, V.D.; Thu, T.V.; Tung, N.Q.; Huy, N.N. Enhanced degradation of organic dyes by peroxymonosulfate with Fe₃O₄-CoCO₃/rGO hybrid activation: A comprehensive study. *J. Taiwan Inst. Chem. Eng.* **2022**, *133*, 104279. [[CrossRef](#)]
93. Li, J.; Lin, Q.; Luo, H.; Fu, H.; Wu, L.; Chen, Y.; Ma, Y. The effect of nanoscale zero-valent iron-loaded N-doped biochar on the generation of free radicals and nonradicals by peroxydisulfate activation. *J. Water Process Eng.* **2022**, *47*, 102681. [[CrossRef](#)]
94. Gu, M.; Farooq, U.; Lu, S.; Zhang, X.; Qiu, Z.; Sui, Q. Degradation of trichloroethylene in aqueous solution by rGO supported nZVI catalyst under several oxidic environments. *J. Hazard. Mater.* **2018**, *349*, 35–44. [[CrossRef](#)]
95. Ahmad, M.; Teel, A.L.; Watts, R.J. Mechanism of persulfate activation by phenols. *Environ. Sci. Technol.* **2013**, *47*, 5864–5871. [[CrossRef](#)]

96. Shang, Y.; Chen, C.; Zhang, P.; Yue, Q.; Li, Y.; Gao, B.; Xu, X. Removal of sulfamethoxazole from water via activation of persulfate by Fe₃C@NCNTs including mechanism of radical and nonradical process. *Chem. Eng. J.* **2019**, *375*, 122004. [[CrossRef](#)]
97. Tian, W.; Zhang, H.; Qian, Z.; Ouyang, T.; Sun, H.; Qin, J.; Tade, M.O.; Wang, S. Bread-making synthesis of hierarchically Co@C nanoarchitecture in heteroatom doped porous carbons for oxidative degradation of emerging contaminants. *Appl. Catal. B-Environ.* **2018**, *225*, 76–83. [[CrossRef](#)]
98. Liang, P.; Zhang, C.; Duan, X.; Sun, H.; Liu, S.; Tade, M.O.; Wang, S. N-Doped Graphene from Metal–Organic Frameworks for Catalytic Oxidation of p-Hydroxybenzoic Acid: N-Functionality and Mechanism. *ACS Sustain. Chem. Eng.* **2017**, *5*, 2693–2701. [[CrossRef](#)]
99. Wang, J.; Duan, X.; Gao, J.; Shen, Y.; Feng, X.; Yu, Z.; Tan, X.; Liu, S.; Wang, S. Roles of structure defect, oxygen groups and heteroatom doping on carbon in nonradical oxidation of water contaminants. *Water Res.* **2020**, *185*, 116244. [[CrossRef](#)]
100. Luo, R.; Li, M.; Wang, C.; Zhang, M.; Khan, M.A.N.; Sun, X.; Shen, J.; Han, W.; Wang, L.; Li, J. Singlet oxygen-dominated non-radical oxidation process for efficient degradation of bisphenol A under high salinity condition. *Water Res.* **2019**, *148*, 416–424. [[CrossRef](#)]
101. Duan, X.; Sun, H.; Shao, Z.; Wang, S. Nonradical reactions in environmental remediation processes: Uncertainty and challenges. *Appl. Catal. B-Environ.* **2018**, *224*, 973–982. [[CrossRef](#)]
102. Yun, E.T.; Yoo, H.Y.; Bae, H.; Kim, H.I.; Lee, J. Exploring the Role of Persulfate in the Activation Process: Radical Precursor Versus Electron Acceptor. *Environ. Sci. Technol.* **2017**, *51*, 10090–10099. [[CrossRef](#)] [[PubMed](#)]
103. Idrees, A.; Shan, A.; Ali, M.; Abbas, Z.; Shahzad, T.; Hussain, S.; Mahmood, F.; Farooq, U.; Danish, M.; Lyu, S. Highly efficient degradation of trichloroethylene in groundwater based on persulfate activation by polyvinylpyrrolidone functionalized Fe/Cu bimetallic nanoparticles. *J. Environ. Chem. Eng.* **2021**, *9*, 105341. [[CrossRef](#)]
104. Li, Z.; Sun, Y.; Huang, W.; Xue, C.; Zhu, Y.; Wang, Q.; Liu, D. Innovatively employing magnetic CuO nanosheet to activate peroxymonosulfate for the treatment of high-salinity organic wastewater. *J. Environ. Sci.* **2020**, *88*, 46–58. [[CrossRef](#)]
105. Soubh, A.M.; Baghdadi, M.; Abdoli, M.A.; Aminzadeh, B. Zero-valent iron nanofibers (ZVINFs) immobilized on the surface of reduced ultra-large graphene oxide (rULGO) as a persulfate activator for treatment of landfill leachate. *J. Environ. Chem. Eng.* **2018**, *6*, 6568–6579. [[CrossRef](#)]
106. Karimipourfard, D.; Eslamloueyan, R.; Mehranbod, N. Heterogeneous degradation of stabilized landfill leachate using persulfate activation by CuFe₂O₄ nanocatalyst: An experimental investigation. *J. Environ. Chem. Eng.* **2020**, *8*, 103426. [[CrossRef](#)]
107. Guo, R.; Meng, Q.; Zhang, H.; Zhang, X.; Li, B.; Cheng, Q.; Cheng, X. Construction of Fe₂O₃/Co₃O₄/exfoliated graphite composite and its high efficient treatment of landfill leachate by activation of potassium persulfate. *Chem. Eng. J.* **2019**, *355*, 952–962. [[CrossRef](#)]
108. Li, Y.; Yuan, X.; Wang, D.; Wang, H.; Wu, Z.; Jiang, L.; Mo, D.; Yang, G.; Guan, R.; Zeng, G. Recyclable zero-valent iron activating peroxymonosulfate synchronously combined with thermal treatment enhances sludge dewaterability by altering physicochemical and biological properties. *Bioresour. Technol.* **2018**, *262*, 294–301. [[CrossRef](#)]
109. Zhang, Y.; Li, T.; Tian, J.; Zhang, H.; Li, F.; Pei, J. Enhanced dewaterability of waste activated sludge by UV assisted ZVI-PDS oxidation. *J. Environ. Sci.* **2022**, *113*, 152–164. [[CrossRef](#)]
110. Liu, C. Enhancement of dewaterability and heavy metals solubilization of waste activated sludge conditioned by natural vanadium-titanium magnetite-activated peroxymonosulfate oxidation with rice husk. *Chem. Eng. J.* **2019**, *359*, 217–224. [[CrossRef](#)]
111. Li, C.; Zhu, Y.; Zhang, T.; Nie, Y.; Shi, W.; Ai, S. Iron nanoparticles supported on N-doped carbon foam with honeycomb microstructure: An efficient potassium peroxymonosulfate activator for the degradation of fluoranthene in water and soil. *Chemosphere* **2022**, *286*, 131603. [[CrossRef](#)]
112. Zhu, Y.; Ji, S.; Liang, W.; Li, C.; Nie, Y.; Dong, J.; Shi, W.; Ai, S. A low-cost and eco-friendly powder catalyst: Iron and copper nanoparticles supported on biochar/geopolymer for activating potassium peroxymonosulfate to degrade naphthalene in water and soil. *Chemosphere* **2022**, *303*, 135185. [[CrossRef](#)]
113. Zhou, Z.; Ma, J.; Liu, X.; Lin, C.; Sun, K.; Zhang, H.; Li, X.; Fan, G. Activation of peroxydisulfate by nanoscale zero-valent iron for sulfamethoxazole removal in agricultural soil: Effect, mechanism and ecotoxicity. *Chemosphere* **2019**, *223*, 196–203. [[CrossRef](#)]
114. Bandala, E.R.; Liu, A.; Wijesiri, B.; Zeidman, A.B.; Goonetilleke, A. Emerging materials and technologies for landfill leachate treatment: A critical review. *Environ. Pollut.* **2021**, *291*, 118133. [[CrossRef](#)]
115. Viegas, C.; Nobre, C.; Mota, A.; Vilarinho, C.; Gouveia, L.; Gonçalves, M. A circular approach for landfill leachate treatment: Chemical precipitation with biomass ash followed by bioremediation through microalgae. *J. Environ. Chem. Eng.* **2021**, *9*, 105187. [[CrossRef](#)]
116. Karimipourfard, D.; Eslamloueyan, R.; Mehranbod, N. Novel heterogeneous degradation of mature landfill leachate using persulfate and magnetic CuFe₂O₄/RGO nanocatalyst. *Process Saf. Environ.* **2019**, *131*, 212–222. [[CrossRef](#)]
117. Maqbool, T.; Cho, J.; Hur, J. Improved dewaterability of anaerobically digested sludge and compositional changes in extracellular polymeric substances by indigenous persulfate activation. *Sci. Total Environ.* **2019**, *674*, 96–104. [[CrossRef](#)]
118. Wang, H.F.; Ma, Y.J.; Wang, H.J.; Hu, H.; Yang, H.Y.; Zeng, R.J. Applying rheological analysis to better understand the mechanism of acid conditioning on activated sludge dewatering. *Water Res.* **2017**, *122*, 398–406. [[CrossRef](#)]
119. Wang, D.; Liu, X.; Zeng, G.; Zhao, J.; Liu, Y.; Wang, Q.; Chen, F.; Li, X.; Yang, Q. Understanding the impact of cationic polyacrylamide on anaerobic digestion of waste activated sludge. *Water Res.* **2018**, *130*, 281–290. [[CrossRef](#)]

120. Wu, B.; Dai, X.; Chai, X. Critical review on dewatering of sewage sludge: Influential mechanism, conditioning technologies and implications to sludge re-utilizations. *Water Res.* **2020**, *180*, 115912. [[CrossRef](#)]
121. Li, Y.; Zhu, Y.; Wang, D.; Yang, G.; Pan, L.; Wang, Q.; Ni, B.J.; Li, H.; Yuan, X.; Jiang, L.; et al. Fe(II) catalyzing sodium percarbonate facilitates the dewaterability of waste activated sludge: Performance, mechanism, and implication. *Water Res.* **2020**, *174*, 115626. [[CrossRef](#)] [[PubMed](#)]
122. Yang, X.; Zeng, L.; Huang, J.; Mo, Z.; Guan, Z.; Sun, S.; Liang, J.; Huang, S. Enhanced sludge dewaterability by a novel MnFe₂O₄-Biochar activated peroxymonosulfate process combined with Tannic acid. *Chem. Eng. J.* **2022**, *429*, 132280. [[CrossRef](#)]
123. Gou, Y.; Zhao, Q.; Yang, S.; Qiao, P.; Cheng, Y.; Song, Y.; Sun, Z.; Zhang, T.; Wang, L.; Liu, Z. Enhanced degradation of polycyclic aromatic hydrocarbons in aged subsurface soil using integrated persulfate oxidation and anoxic biodegradation. *Chem. Eng. J.* **2020**, *394*, 125040. [[CrossRef](#)]